

# 1. GEOCHEMISTRY AND GEOCHRONOLOGY OF LEG 130 BASEMENT LAVAS: NATURE AND ORIGIN OF THE ONTONG JAVA PLATEAU<sup>1</sup>

John J. Mahoney,<sup>2</sup> Michael Storey,<sup>3</sup> Robert A. Duncan,<sup>4</sup> Khalil J. Spencer,<sup>2</sup>  
and Malcolm Pringle<sup>5</sup>

## ABSTRACT

Basement rocks from the Ontong Java Plateau are tholeiitic basalts that appear to record very high degrees of partial melting, much like those found today in the vicinity of Iceland. They display a limited range of incompatible element and isotopic variation, but small differences are apparent between sampled sites and between upper and lower groups of flows at Ocean Drilling Program Site 807. <sup>40</sup>Ar-<sup>39</sup>Ar ages of lavas from Site 807 and Deep Sea Drilling Project Site 289 are indistinguishable about an early Aptian mean of 122 Ma (as are preliminary data for the island of Malaita at the southern edge of the plateau), indicating that plateau-building eruptions ended more or less simultaneously at widely separated locations. Pb-Nd-Sr isotopes for lavas from Sites 289, 803, and 807, as well as southern Malaita, reflect a hotspot-like source with  $\epsilon_{Nd}(T) = +4.0$  to  $+6.3$ ,  $(^{87}Sr/^{86}Sr)_T = 0.70423-0.70339$ , and  $^{206}Pb/^{204}Pb = 18.245-18.709$  and possessing consistently greater  $^{206}Pb/^{204}Pb$  for a given  $^{206}Pb/^{204}Pb$  than Pacific MORB. The combination of hotspot-like mantle source, very high degrees of melting, and lack of a discernible age progression is best explained if the bulk of the plateau was constructed rapidly above a surfacing plume head, possibly that of the Louisville hotspot.

Basalt and feldspar separates indicate a substantially younger age of ~90 Ma for basement at Site 803; in addition, volcanoclastic layers of mid-Cenomanian through Coniacian age occur at DSDP Site 288, and beds of late Aptian-Albian age are found at Site 289. Therefore, at least some volcanism continued on the plateau for 30 m.y. or more. The basalts at Site 803 are chemically and isotopically very similar to those at the ~122 Ma sites, suggesting that hot plume-type mantle was present beneath the plateau for an extended period or at two different times.

Surviving seamounts of the Louisville Ridge formed between 70 and 0 Ma have much higher  $^{206}Pb/^{204}Pb$  than any of the plateau basalts. Thus, assuming the Louisville hotspot was the source of the plateau lavas, a change in the hotspot's isotopic composition may have occurred between roughly 70 and 90 Ma; such a change may have accompanied the plume-head to plume-tail transition. Similar shifts from early, lower  $^{206}Pb/^{204}Pb$  to subsequently higher  $^{206}Pb/^{204}Pb$  values are found in several other oceanic plateau-hotspot and continental flood basalt-hotspot systems, and could reflect either a reduction in the supply of low  $^{206}Pb/^{204}Pb$  mantle or an inability of some off-ridge plume-tails to melt refractory low  $^{206}Pb/^{204}Pb$  material.

## INTRODUCTION

Oceanic plateaus are extensive volcanic constructional features with crustal thicknesses of ~18–40 km (Hussong et al., 1979) that occur in all three major ocean basins. Despite their often immense size, their origins are understood poorly, in large part because of a dearth of basement sampling and, hence, of information on age and mantle sources. In the Pacific, by far the best sampled of these features at present is the Ontong Java Plateau (Fig. 1), where recent drilling during Ocean Drilling Program (ODP) Leg 130 penetrated 149 m of basement at Site 807 and 26 m at Site 803 (Kroenke, Berger, Janecek, et al., 1991). Before Leg 130, the submarine crust of the plateau was known only from a single, altered basalt flow drilled at Deep Sea Drilling Project (DSDP) Site 289 (e.g., Stoesser, 1975). Some probable plateau basement also is exposed subaerially at the southwestern edge of the plateau on the islands of Malaita and Small Malaita; although we have completed preliminary geochemical work and age determinations on a collection of Malaitan rocks, comprehensive studies are still underway. In this paper we present chemical Nd-Sr-Pb isotopic and <sup>40</sup>Ar-<sup>39</sup>Ar geochronological data for the Leg 130 lavas and use

the results to address the petrogenesis, timing, and environment of the plateau's formation.

Combined geochemical, gravity, and plate-tectonic evidence indicates that most of the Pacific plateaus may have been formed above near-ridge or ridge-centered Cretaceous hotspots (Mahoney, 1987). At least the largest ones may reflect the arrival at the base of the lithosphere (not necessarily near ridges) of the inflated "heads" of new mantle plumes (Richards et al., 1989); this plume-initiation hypothesis predicts plateau-forming volcanism to be cataclysmic in nature, beginning suddenly and lasting only a few million years. In contrast, plateaus created at robust but more or less steady-state near-ridge hotspots—that is, plume "tails"—could take tens of millions of years to form, their size depending upon both the size of the hotspot and the rate of plate movement relative to the hotspot (Mahoney and Spencer, 1991). The medium-sized Icelandic Plateau (~250,000 km<sup>2</sup>) in the North Atlantic is an example of the latter type, having been created near the slowly spreading Mid-Atlantic Ridge over a period of at least 25 m.y. by the already mature Icelandic hotspot (e.g., Oskarsson et al., 1985). At present, the best evidence for the plume-initiation mechanism is found in the probable continental analogs of many oceanic plateaus; namely, large continental flood basalt provinces. Recent high-precision <sup>40</sup>Ar-<sup>39</sup>Ar dating in the Siberian (Renne and Basu, 1991), Deccan (Duncan and Pyle, 1988; Courtillot et al., 1988), and Columbia River (e.g., Baksi, 1989) provinces, for example, indicates that enormous portions of each were formed in only 1–2 m.y., or even less. Because of the considerable influence large, initial plume-heads should exert on rift propagation, plume heads in oceanic areas are likely to become associated with spreading centers even if they first appear in a location distant from a ridge (Mahoney and Spencer, 1991); thus, the plume-initiation and near-ridge hotspot concepts need not be mutually exclusive. A third

<sup>1</sup> Berger, W.H., Kroenke, L.W., Mayer, L.A., et al., 1993. *Proc. ODP, Sci. Results*, 130: College Station, TX (Ocean Drilling Program).

<sup>2</sup> Department of Geology and Geophysics, School of Ocean and Earth Science and Technology, University of Hawaii, 2525 Correa Road, Honolulu, HI 96822, U.S.A.

<sup>3</sup> Department of Geology, University of Keele, Staffordshire ST5 5BH, United Kingdom (present address: Department of Geology, University of Leicester, Leicester LE1 7RH, United Kingdom).

<sup>4</sup> College of Oceanography, Oregon State University, Corvallis, OR 97331, U.S.A.

<sup>5</sup> Branch of Isotope Geology, U.S. Geological Survey, 345 Middlefield Road, Menlo Park, CA 94025, U.S.A.

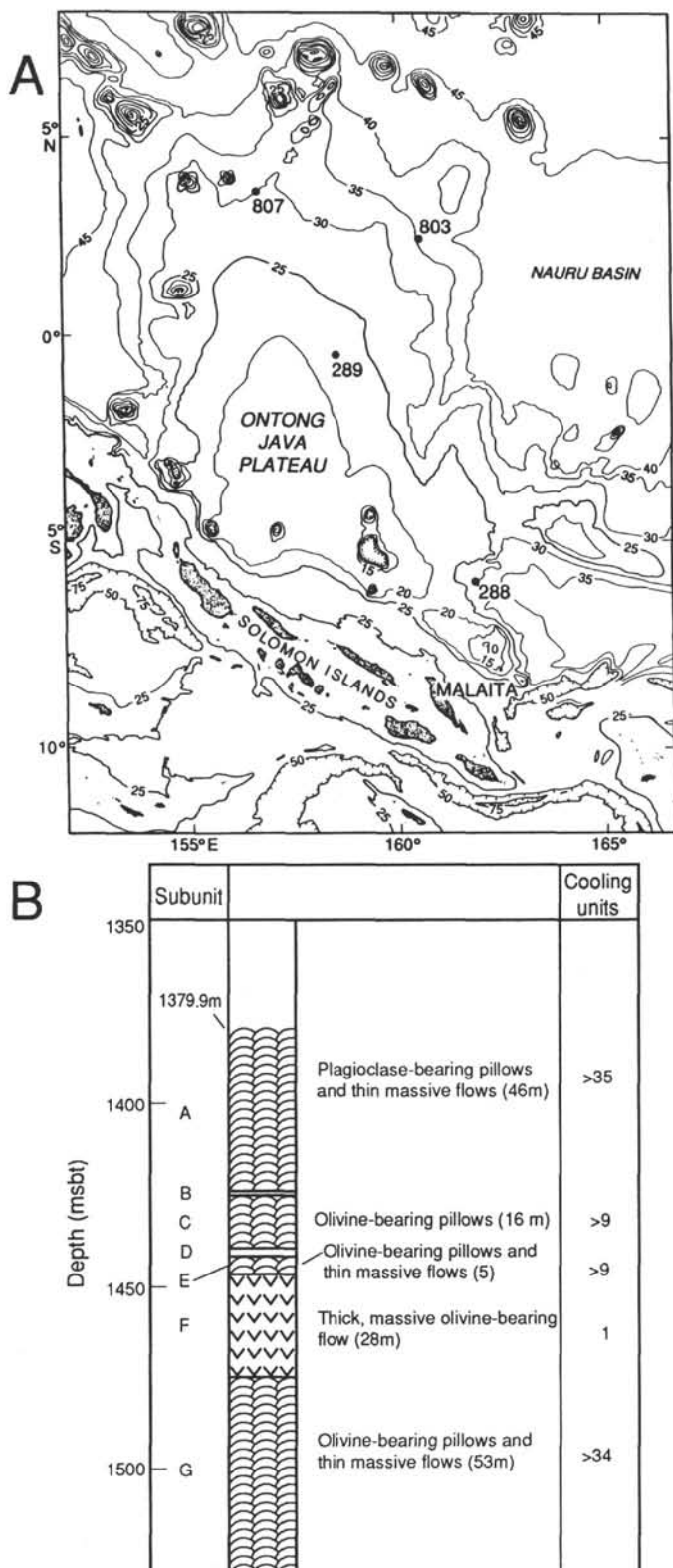


Figure 1. A. Map of the main part of the Ontong Java Plateau, showing locations of Leg 130 Sites 803 and 807, DSDP Sites 288 (which did not reach basement) and 289, and the island of Malaita. Bathymetric contour interval is 2500 m; additional contours have been added (at 500-m intervals) on and near the plateau to illustrate its morphology. B. Lithologic column of basement at Site 807, illustrating unit thickness and estimated number of cooling units (individual massive or pillowed flows) in each. Units B and D are sedimentary interbeds.

hypothesis proposed recently for the Pacific plateaus views them all as manifestations of a single gigantic “superplume” that originated at the core-mantle boundary, surfaced in the Early Cretaceous, and largely spent itself by 100 Ma (Larson, 1991). In this case, the Pacific plateaus may not be associated with specific present-day hotspots.

The two largest oceanic plateaus in the world are the Ontong Java ( $>1.5 \times 10^6 \text{ km}^2$ ) and the Kerguelen Plateau–Broken Ridge pair (with nearly as great an extent) in the southeastern Indian Ocean. Apart from their great size, these two plateaus are significantly different. For example, the Kerguelen Plateau was formed in a new ocean basin, in close proximity to rifting continental lithosphere, just after the breakup of Indo-Madagascar from Antarctica-Australia; this factor makes it difficult in studies of the plateau lavas to distinguish geochemical characteristics inherited from sublithospheric mantle sources from those caused by the influence of mobilized Gondwanan lithosphere (e.g., Storey et al., 1989, 1992). In contrast, available evidence indicates that the Ontong Java Plateau originated in an intraoceanic setting, far away from any sizable continental mass (e.g., Yan and Kroenke, this volume); thus, interpretation of Ontong Java geochemical signatures can be made with much less concern about direct continental lithospheric contributions. On the other hand, although nearly all workers consider the Kerguelen Plateau to be the early product of the present Kerguelen hotspot (e.g., Duncan, 1991), the identity of any hotspot responsible for the formation of the Ontong Java Plateau is much less certain. Plate reconstructions of the paleo-Pacific suggest that the Louisville hotspot (50°S, 139°W) may have played a key role (e.g., Richards et al., 1989; Mahoney and Spencer, 1991; Tarduno et al., 1991), but the connection has remained speculative because of a lack of data on Ontong Java basement age, large uncertainties in pre-90-Ma Pacific reconstructions, as well as pronounced geochemical differences between the few basement lavas analyzed previously and volcanic rocks of the Louisville Ridge, the 0–70 Ma trace of the hotspot.

## GEOCHRONOLOGY

### Samples and Methods

Shipboard descriptions of the Site 803 and 807 basement rocks have been given by Kroenke, Berger, Janecek, et al. (1991). Briefly, basement recovered at both sites consists of sparsely porphyritic to aphyric tholeiitic basalts. Those at Site 807 have been subdivided into five stratigraphic units or packets of flows, labeled A, C, E, F, G (Units B and D are sedimentary interbeds); Unit F is a single 28-m-thick massive flow (Fig. 1B). Several thin, pillowed lavas, all classified as one stratigraphic unit, were drilled at Site 803. At Site 807, flows comprising igneous Units C–G contain sparse, ~0.5-mm diameter olivine phenocrysts, extensively altered to dark green clay. These are lacking in Unit A lavas, as well as in the Site 803 basalts, which instead possess rare, relatively fresh plagioclase phenocrysts (two examples of fresh, subhedral grains ~5 mm to 1 cm across were observed). The Site 807 basalts vary from quite fresh to moderately altered in hand specimen and thin section, displaying medium-gray groundmasses and <10% to ~30% total alteration. Groundmass plagioclase and clinopyroxene are relatively fresh, but mesostasis is variably altered to clays, and in places veins containing celadonite, calcite, and possibly zeolites are present. Basalts from Site 803 range from moderately to highly altered, with gray to brownish gray groundmasses and roughly 25%–50% alteration of mesostasis and groundmass phases. Alteration in the DSDP Site 289 flow (Stoeser, 1975) is comparable with that in some of our more altered Site 803 specimens.

In an attempt to establish the space-time relationships of volcanism across the plateau,  $^{40}\text{Ar}$ – $^{39}\text{Ar}$  incremental heating methods were employed. Because seawater alteration of primary igneous phases (olivine, pyroxene, feldspar, oxides, glass) to clays, zeolites, celadonite, and calcite causes loss of radiogenic  $^{40}\text{Ar}$  and addition of K, standard K–Ar radiometric dates usually seriously underestimate

the crystallization age of altered samples. The  $^{40}\text{Ar}$ - $^{39}\text{Ar}$  method is a variation of K-Ar chronometry that relies on neutron irradiation of samples to produce  $^{39}\text{Ar}$  from  $^{39}\text{K}$ . Subsequent incremental heating of the sample under vacuum allows extraction of parent ( $^{39}\text{Ar}$ , representing K) and daughter ( $^{40}\text{Ar}$ ) isotopes from discrete temperature steps. Alteration phases are less retentive of Ar because of their open structures, so Ar diffuses out of them at low temperatures. In fact, much of the K added from seawater probably resides on grain boundaries, in vesicles and cracks, and  $^{39}\text{Ar}$  formed from it will be lost from the sample during irradiation. Conversely, the remaining igneous phases outgas at higher temperatures, and their Ar isotopic compositions reflect the desired crystallization age of the sample. Hence, it is often possible to separate the contributions of alteration and igneous phases to the sample's total Ar isotopic composition.

For the samples studied here, pieces of cored basalt were trimmed to obtain the freshest and best crystallized material. These samples were crushed to 0.5–1 mm size, handpicked to remove vein alteration, and ultrasonically washed in distilled water. Approximately 0.5-g splits of the prepared whole-rock chips were sealed in evacuated quartz tubes and irradiated for 6–8 hr in the core of the Oregon State University TRIGA reactor, where they received a neutron dose of  $\sim 0.7 \times 10^{18}$  nvt. The efficiency of conversion of  $^{39}\text{K}$  to  $^{39}\text{Ar}$  by neutron capture was monitored with samples of hornblende standard Mmhb-1 (520.4  $\pm$  1.7 Ma; Samson and Alexander, 1987). Further details of the flux characteristics, monitor minerals, and corrections for interfering K- and Ca-derived Ar isotopes are reported by Dalrymple et al. (1981).

Argon extractions were performed at Oregon State University in a conventional high-vacuum glass line using radio-frequency induction heating. Heating steps were set from power levels on the generator and were determined from previous experience to divide the total whole-rock Ar into five or six roughly equal portions. Samples were held at each temperature-step setting for 30 min, and the Ar composition of each gas increment was measured mass spectrometrically with an AEI MS-10S instrument with computer-controlled peak switching and data acquisition. The system background (blank) was  $3 \times 10^{-14}$  moles  $^{40}\text{Ar}$ .

In addition, megacrystic (0.5–1 cm) plagioclase feldspars were separated from two samples of Site 803 basalts. These were acid-

treated (in HCl and HF), washed and dried, and irradiated in the U.S. Geological Survey's TRIGA reactor under similar conditions as the whole-rock chips. Argon extractions were performed at the U.S. Geological Survey (Menlo Park) using a 5W Ar-ion laser-probe connected directly with a MAP 216 mass spectrometer. Preheating of the samples (each  $\sim 1$  mg in size) using an unfocused laser beam ( $\sim 600^\circ\text{C}$ ) removed most surficial atmospheric  $^{40}\text{Ar}$ . Step-heating was achieved in six increments by increasing power to the focused laser beam until sample fusion. Typical step-gas compositions were more than 50% radiogenic  $^{40}\text{Ar}$ . The system background was  $< 1 \times 10^{-15}$  moles  $^{40}\text{Ar}$ . The reactor flux monitor (J) was measured with the 27.92 Ma sanidine standard 85G003 from the Taylor Creek rhyolite; this is equivalent to an age of 513.9 Ma for the Mmhb-1 hornblende standard. To enable a direct comparison between the Oregon State and USGS data, the results for the Site 803 plagioclases have been recalculated to be equivalent to a 520.4 Ma age for Mmhb-1.

## Results

Results from our  $^{40}\text{Ar}$ - $^{39}\text{Ar}$  incremental heating experiments are reported in Table 1, and representative examples are illustrated in Figures 2–5. Data are displayed in age-spectra diagrams, in which the ages calculated from the composition of gas in each heating step for a given sample are plotted against cumulative gas released ( $\%^{39}\text{Ar}$ ). In most samples (e.g., Fig. 2A), concordant ages for middle- to high-temperature steps define a plateau age, which provides the best estimate of the age of rock crystallization (note that such a plateau is a *type* of  $^{40}\text{Ar}$ - $^{39}\text{Ar}$  age, not the age of an oceanic plateau sample). Gas compositions for the various steps also can be correlated in isotope-ratio diagrams (e.g., Fig. 2B) where colinear points are fitted by least squares to yield a slope, which determines an isochron age, and an intercept, which defines the composition of Ar in the sample when it crystallized (expected to be atmospheric,  $^{40}\text{Ar}/^{36}\text{Ar} = 295.5$ ). Unlike the age-spectra plots, which assume an initial  $^{40}\text{Ar}/^{36}\text{Ar}$  composition equal to the atmospheric ratio, isotope correlation diagrams allow independent determination of sample age and initial  $^{40}\text{Ar}/^{36}\text{Ar}$ . The goodness-of-fit parameter SUMS (York, 1969) has a  $\chi^2$  distribution with  $N - 2$  degrees of freedom,  $N$  being the number of steps included

Table 1.  $^{40}\text{Ar}$ - $^{39}\text{Ar}$  plateau and isochron ages for basaltic rocks from the Ontong Java Plateau.

Core, section, interval (cm)	Plateau age $\pm 1 \sigma$ (Ma)	Integrated age (Ma)	$^{39}\text{Ar}$ (% of total)	Isochron age $\pm 1 \sigma$ (Ma)	SUMS ( $N - 2$ )	$^{40}\text{Ar}/^{36}\text{Ar}$ intercept
Oregon State University:						
130-807C-						
75R-2, 129–131	121.0 $\pm$ 4.5	118.8	80	121.7 $\pm$ 3.6	0.08	297.3 $\pm$ 11.0
78R-1, 67–69	121.4 $\pm$ 1.9	124.1	75	124.0 $\pm$ 2.5	0.40	294.0 $\pm$ 3.3
79R-1, 17–18	None developed	98.7	—	None	—	—
80R-1, 52–55	119.9 $\pm$ 2.6	118.2	100	122.4 $\pm$ 4.0	1.22	290.5 $\pm$ 4.9
84R-6, 0–3	123.4 $\pm$ 2.5	124.5	97	122.6 $\pm$ 1.7	0.05	292.6 $\pm$ 17.5
90R-1, 38–41	124.7 $\pm$ 2.2	126.3	100	119.5 $\pm$ 9.9	0.28	307.6 $\pm$ 29.9
93R-3, 15–18	122.1 $\pm$ 2.2	143.9	68	126.0 $\pm$ 4.8	0.30	294.0 $\pm$ 3.0
130-803D-						
71R-1, 114–115	None developed	55.5	—	None	—	—
71R-2, 87–88	88.2 $\pm$ 1.1	88.3	99	85.7 $\pm$ 1.3	0.49	294.7 $\pm$ 2.6
30-289-						
132-4, 79–81	121.7 $\pm$ 2.7	121.0	100	128.5 $\pm$ 2.6	0.53	288.8 $\pm$ 4.1
132-4, 122–125	122.8 $\pm$ 2.4	121.4	100	122.7 $\pm$ 2.2	0.22	293.0 $\pm$ 3.1
U.S. Geological Survey:						
130-803D-						
69R-1, 87–89	86.1 $\pm$ 4.6	86.1	100	83.1 $\pm$ 2.5	1.03	483 $\pm$ 117
71R-1, 14–16	83.7 $\pm$ 3.1	84.2	100	82.7 $\pm$ 1.5	0.16	304.9 $\pm$ 14.6
	93.9 $\pm$ 1.4*	93.6	100	93.8 $\pm$ 2.8	1.06	296.2 $\pm$ 9.8

\*Weighted mean of six total-fusion analyses of  $\sim 1$  mg crystals; corresponding isochron age from colinear total-fusion gas compositions.

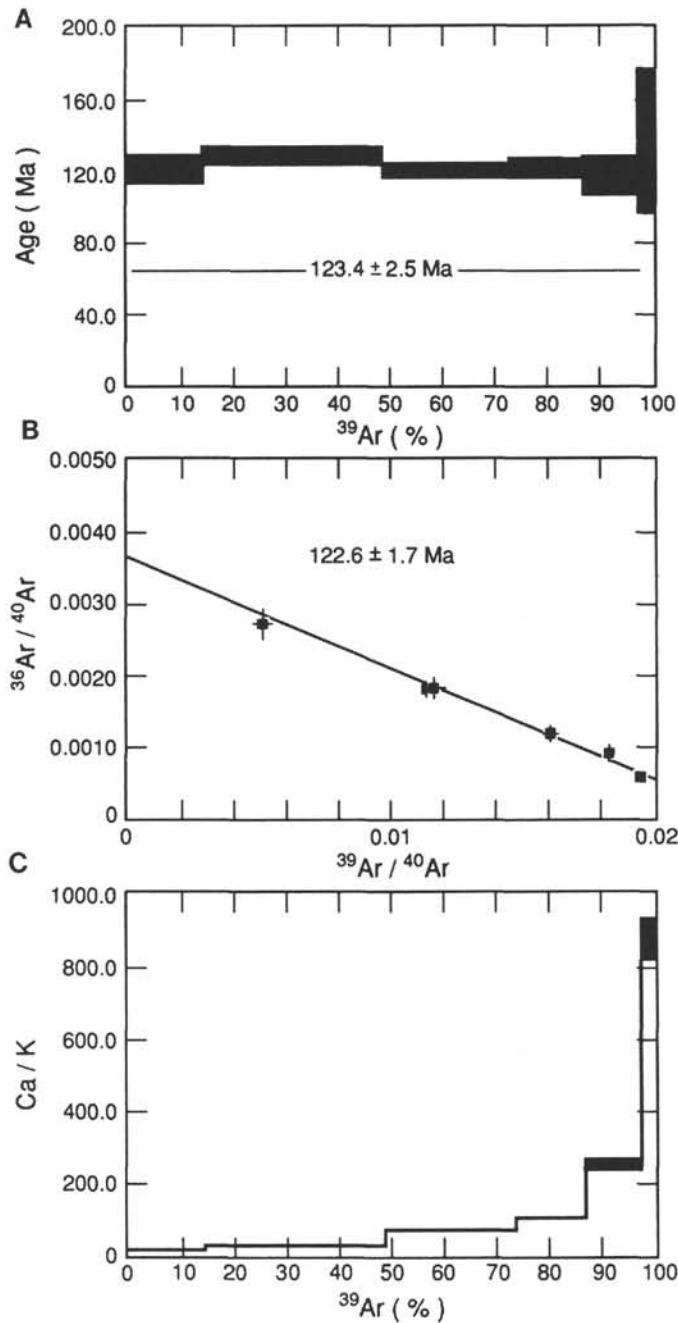


Figure 2. A. Apparent age-release diagram for  $^{40}\text{Ar}$ - $^{39}\text{Ar}$  incremental heating experiment on basalt Sample 130-807C-84R-6, 0–3 cm. Horizontal bars indicate estimated analytical error ( $\pm 1\sigma$ ) about each step age. A plateau age (indicated) has been determined from the weighted mean of contiguous, concordant step ages. B.  $^{36}\text{Ar}/^{40}\text{Ar}$  vs.  $^{39}\text{Ar}/^{40}\text{Ar}$  isotope correlation diagram for the step Ar compositions measured. The isochron age (indicated) is calculated from the best-fitting line through colinear step compositions, after York (1969); analytical uncertainties are shown. C. Ca/K values inferred from step Ar compositions reflect the phases (pyroxene, feldspar, groundmass, clays) contributing to gas released at each temperature.

in the linear regression. In Table 1, the F-variate statistic  $\text{SUMS}/(N-2)$  (i.e., the ratio of total scatter about the isochron to the scatter attributable to analytical error alone) is given. For reference, a value of  $\text{SUMS}/(N-2) = 2.6$  for a regression fitted with five plateau steps would indicate that an isochron relationship could not be dismissed at the 95% confidence limit. Experiments that yield such an accept-

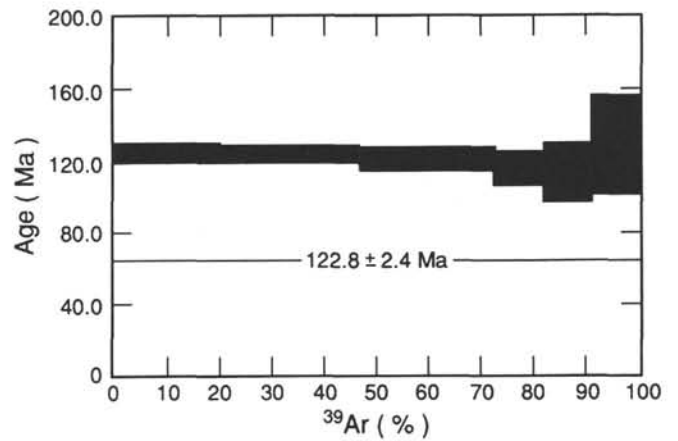


Figure 3. Apparent age-release diagram for  $^{40}\text{Ar}$ - $^{39}\text{Ar}$  incremental heating experiment of DSDP basalt Sample 30-289-132-4, 122–125 cm. Details as in Figure 2A.

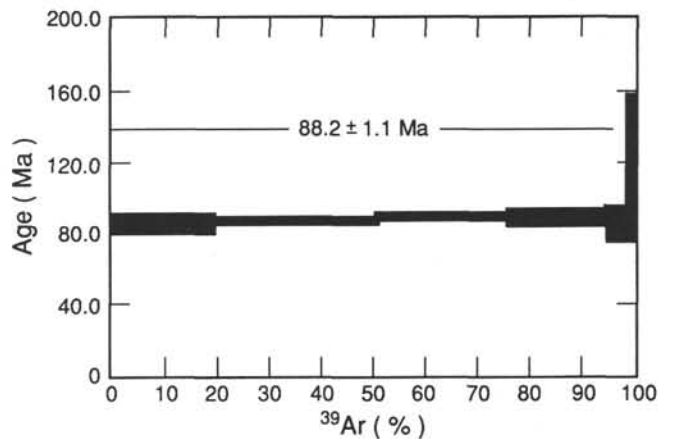


Figure 4. Apparent age-release diagram for  $^{40}\text{Ar}$ - $^{39}\text{Ar}$  incremental heating experiment of basalt Sample 130-803D-71R-2, 87–88 cm. Details as in Figure 2A.

able measure of goodness of fit, an atmospheric  $^{40}\text{Ar}/^{36}\text{Ar}$  intercept, and concordant isochron and plateau ages define reliable crystallization ages (Lanphere and Dalrymple, 1978).

In addition to age determination, the Ca/K of individual steps can be calculated from Ar isotopic compositions using  $1.852 \times ^{37}\text{Ar}/^{39}\text{Ar}$  (Walker and McDougall, 1982); the phases outgassing at each step then can be identified from known Ca/K ratios for different minerals: 500–2000 for clinopyroxene, 20–500 for plagioclase, 1–20 for basaltic groundmasses, and  $<1$  for clays. Plots of Ca/K vs.  $\%^{39}\text{Ar}$  for our experiments (e.g., Fig. 2C) show that Ca/K increased with temperature from values of  $\sim 10$  to  $\sim 100$ . The temperature steps that define the plateau ages in Table 1, therefore, are associated primarily with Ca/K appropriate for groundmass and plagioclase feldspars.

#### Discussion and Interpretation of Age Determinations

The incremental heating experiments produced variably disturbed age spectra; most, like the examples illustrated in the figures, developed nearly ideal plateaus comprising over 90% of the total Ar in the samples. Spurious step ages generally resulted from small amounts of gas released at low temperatures, which we attribute to nonconcordant loss of radiogenic  $^{40}\text{Ar}$  (during alteration) and  $^{39}\text{Ar}$  (during irradiation) from alteration minerals. Plateau ages, defined by three or more concordant step ages making up more than 50% of the total

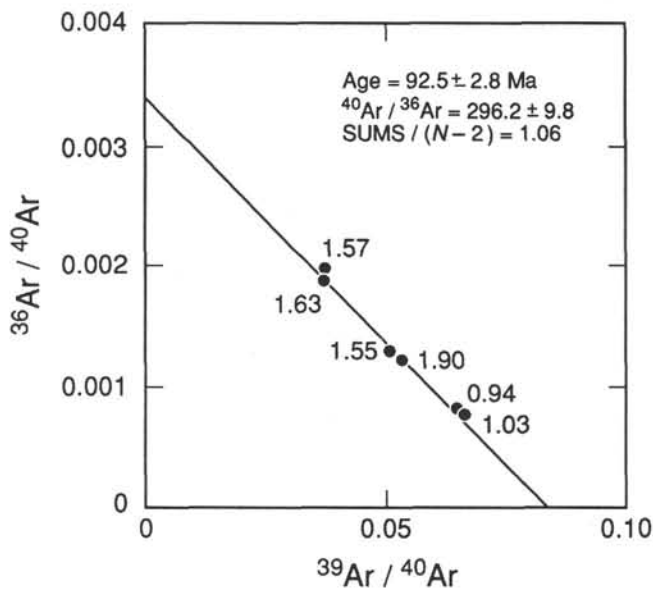


Figure 5.  $^{36}\text{Ar}/^{40}\text{Ar}$  vs.  $^{39}\text{Ar}/^{40}\text{Ar}$  isotope correlation diagram for feldspar separated from basalt Sample 130-803D-71R-1, 14–16 cm. Details as in Figure 2B, except points are total-fusion Ar compositions of individual crystals (weights of which are given in milligrams).

Ar, were calculated as the mean of the step ages (weighted inversely by their variances). An integrated sample age was calculated by adding together all the step compositions; this age should be equivalent to an  $^{40}\text{Ar}/^{39}\text{Ar}$  total-fusion age. Isochron ages were determined from the slope of the best-fit line through the isotopic values of the plateau-defining steps. For all of our samples,  $^{40}\text{Ar}/^{36}\text{Ar}$  intercepts were near the atmospheric value; for the Site 807 basalts, at least, this is not surprising in view of the evidence from Unit B (a limestone interbed) that they were erupted above the calcite compensation depth (Kroenke, Berger, Janecek, et al., 1991).

Six whole-rock samples from Site 807 yield crystallization ages indistinguishable from one another, with a weighted mean plateau value of  $122.3 \pm 1.0$  Ma, corresponding to an early Aptian age (e.g., Harland et al., 1990). The presence of Aptian microfossils in sediments overlying and interbedded with these basalts is compatible with this age (Kroenke, Berger, Janecek, et al., 1991). Paleomagnetic data (Tarduno et al., 1991) show that all of the basalts and overlying limestones are normally magnetized, and it is likely that they were magnetized during the earliest part of the long Cretaceous interval of normal polarity. In fact, our new age determinations provide the best minimum estimate available for the age of M0, the last reversal before the long normal interval, and for the Aptian/Barremian boundary.

Two samples from the basement flow at DSDP Site 289 (located over 500 km from Site 807) were analyzed at the same time as the Leg 130 lavas; they also produced good results. Significantly, their plateau ages are identical to those at Site 807 (Table 1 and Fig. 3). Sample 30-289-132-4, 79–81 cm, is the single instance of discordant plateau and isochron ages; its  $^{40}\text{Ar}/^{36}\text{Ar}$  intercept (288.8) is slightly lower than the atmospheric value. We see no evidence to conclude that the initial Ar composition in this sample was nonatmospheric; rather, the low intercept is an artifact of the grouping of step-gas compositions. Hence, the isochron age for this sample is somewhat too old and we prefer the plateau age ( $121.7 \pm 2.7$  Ma). Remarkably, basalts of similar chemical composition to the Site 289 and Site 807 lavas upthrust on the island of Malaita yield identical  $^{40}\text{Ar}/^{39}\text{Ar}$  incremental heating ages (122–123 Ma; R.A. Duncan, unpubl. data, 1991).

Two whole-rock and two feldspar samples from Site 803 were analyzed (Table 1 and Figs. 4–5); good plateau ages were obtained

for three of them. The feldspar sample from 130-803D-71R-1, 14–16 cm, was run in two laser-heating modes: in the first, incremental heating produced a plateau age of  $83.7 \pm 3.1$  Ma (six steps), whereas in the second a series of total-fusion measurements on six ~1-mg crystals gave a weighted mean age of  $93.9 \pm 1.4$  Ma. Corresponding isochron ages are similar. Petrographically, the second mineral fraction, which gave the greater age, was fresher (i.e., translucent, euhedral crystals vs. more opaque ones in the first case). Although it is conceivable that the more altered grains of the first fraction record a postmagmatic recrystallization event some 8–10 m.y. younger than the volcanism at Site 803, no evidence is present to indicate this; the Ca/K values of feldspars in the two fractions are virtually identical (in the 100–1000 range), with no hint of K-feldspar overgrowths. Argon loss in the more altered crystals could explain the age difference, but we see no evidence of an older igneous age in the higher temperature steps. The whole-rock age ( $88.2 \pm 1.1$  Ma) falls within the range of the feldspar ages. A possible mid-Cenomanian age for the lowermost sediments at this site (Kroenke, Berger, Janecek, et al., 1991) is most compatible with the older of the feldspar ages. Regardless of the precise crystallization age of the Site 803 basalts, it is clear that volcanism at this location occurred about 30 m.y. after the formation of basement (strictly, the termination of volcanism) at Sites 807 and 289, and apparently, in southern Malaita.

## GEOCHEMISTRY

### Samples and Methods

The Leg 130 samples analyzed here were chosen on board ship by the two senior authors on the basis of relative freshness and representative coverage of section—not always compatible goals, particularly near the more altered top of basement at both sites. Major elements and Rb, Zr, Sr, Y, V, Cr, and Ni were measured on agate- or alumina-ground bulk-sample (free of obvious veins) powders by standard X-ray fluorescence methods at the University of Keele. Trace elements were analyzed on powder briquets and major elements on fused disks consisting of a mixture (by weight) of one part sample powder to five parts  $\text{LiBO}_2$  flux. Further information on methodology is given by Floyd (1986). Our results appear in Table 2 along with estimated analytical uncertainties.

Nine lanthanide rare-earth elements plus Th, Ta, Hf, and Sc were determined on 0.2-g splits of ten of the powders by instrumental neutron activation analysis at the University of Leicester following Saunders (1986). In addition, neutron activation data were obtained for a sample from the flow at DSDP Site 289, as well as for two Manihiki Plateau basalts from Site 317. Splits of 21 powders were analyzed for Cs, Rb, Ba, Th, U, Nb, Ta, Zr, Hf, Y, Sc, and rare-earth elements by inductively coupled plasma-mass spectrometry at the University of Durham. For each sample, 0.1 g of powder was dissolved (with HF,  $\text{HClO}_4$ , and  $\text{HNO}_3$ ), spiked with Rh and Re internal standards, and run on a VG Plasmaquad instrument in a dilute  $\text{HNO}_3$  matrix (i.e., ~0.1 g total dissolved solids; total dilution factor = 500) with a dwell time of 250 s for each element analyzed. Correction procedures included drift monitoring and subtraction of blank contributions, oxide and hydroxide interferences, and overlap of neighboring isotopes on the peaks of interest. Calibration was effected by synthetic standards checked against a set of laboratory and international standards. Table 3 lists both the neutron activation and plasma-mass-spectrometric data, along with estimated analytical uncertainties. Splits of five samples were analyzed by both methods; in general, values for elements determined by both techniques are in good agreement (Sc shows by far the most variability). Also, comparison of Tables 2 and 3 shows that agreement between X-ray fluorescence and plasma-mass-spectrometric data is good for Rb and excellent for Zr and Y, the three elements analyzed in common.

Isotopic ratios of Nd, Sr, and Pb, as well as isotope-dilution abundances of Nd, Sm, Sr, Rb, and Pb (Tables 4 and 5) were measured in the Isotope Laboratory at the University of Hawaii,

Table 2. Major element and X-ray fluorescence trace element data for Leg 130 basalts.

Core, section, interval (cm)	SiO <sub>2</sub>	TiO <sub>2</sub>	Al <sub>2</sub> O <sub>3</sub>	Fe <sub>2</sub> O <sub>3</sub> *	MnO	MgO	CaO	Na <sub>2</sub> O	K <sub>2</sub> O	P <sub>2</sub> O <sub>5</sub>	LOI	Total	Cr	Ni	Rb	Sr	V	Y	Zr
130-807C-																			
Unit A																			
74R-1, 46-49	47.12	1.70	15.09	14.05	0.14	4.77	12.24	2.37	0.76	0.16	1.77	100.2	168	94	15	250	365	32	101
74R-1, 124-127	48.65	1.66	14.73	12.54	0.18	6.05	12.43	2.45	0.41	0.14	0.66	99.9	170	96	10	218	331	30	102
74R-2, 118-122	48.55	1.61	14.23	13.01	0.22	6.82	12.12	2.46	0.14	0.14	0.59	99.9	164	99	<4	203	327	30	98
74R-3, 86-90	48.65	1.59	14.09	13.45	0.20	7.28	11.82	2.40	0.09	0.14	0.25	100.0	150	95	<4	177	310	30	100
74R-4, 8-12	48.60	1.60	14.11	13.42	0.19	7.10	11.84	2.25	0.08	0.14	0.45	99.8	151	98	<4	183	309	29	98
75R-1, 27-30	47.31	1.52	13.45	14.00	0.19	6.51	12.06	2.21	0.84	0.14	1.69	99.9	154	72	28	182	322	29	94
75R-2, 61-64	48.17	1.59	14.07	13.51	0.20	7.26	11.77	2.32	0.35	0.14	0.62	100.0	154	115	8	198	327	29	99
75R-2, 125-129	48.26	1.63	14.51	13.00	0.19	7.20	12.16	2.34	0.05	0.14	0.50	100.0	149	100	<4	210	314	31	101
75R-3, 104-107	48.69	1.59	14.26	13.30	0.19	6.79	11.91	2.33	0.13	0.14	0.35	99.7	160	98	<4	178	314	30	99
75R-4, 48-52	48.75	1.62	14.16	13.43	0.21	6.74	12.13	2.38	0.13	0.14	0.45	100.1	162	99	<4	174	313	30	98
75R-5, 78-83	48.85	1.60	14.22	13.39	0.19	7.03	11.87	2.38	0.13	0.14	0.18	100.0	159	97	<4	170	315	31	100
76R-1, 69-71	49.06	1.61	14.35	13.33	0.18	6.42	11.94	2.43	0.12	0.13	0.20	99.8	156	100	<4	173	325	30	99
77R-1, 48-51	48.88	1.61	14.33	13.27	0.19	6.70	11.99	2.49	0.13	0.14	0.27	100.0	153	99	<4	172	316	29	99
78R-1, 63-67	49.01	1.60	14.28	13.37	0.19	7.25	11.89	2.43	0.09	0.14	0.20	100.5	154	96	<4	165	299	29	98
78R-2, 69-72	48.76	1.59	14.05	13.49	0.27	7.18	11.75	2.34	0.31	0.14	0.40	100.3	143	95	6	166	305	30	97
78R-3, 55-60	49.14	1.62	14.28	13.53	0.19	6.72	12.19	2.42	0.11	0.14	0.13	100.5	157	95	6	170	333	29	98
79R-1, 13-17	48.83	1.61	14.22	13.29	0.19	6.84	12.17	2.40	0.10	0.14	0.28	100.1	156	94	7	171	324	29	98
79R-3, 110-114	48.31	1.61	14.42	13.53	0.23	6.90	12.12	2.40	0.30	0.14	0.07	100.0	162	86	12	173	358	28	98
79R-4, 25-28	47.55	1.60	13.89	14.86	0.22	6.97	11.94	2.32	0.38	0.14	0.27	100.1	160	78	15	166	349	29	98
79R-5, 28-30	49.46	1.65	14.62	12.75	0.18	6.45	12.30	2.49	0.11	0.14	0.41	100.6	150	97	<4	175	332	31	102
79R-5, 34-38	48.67	1.60	14.51	12.67	0.18	6.72	12.40	2.45	0.08	0.14	0.47	99.9	153	105	6	184	327	28	98
80R-1, 49-51	48.44	1.66	14.79	12.77	0.40	7.02	12.27	2.41	0.07	0.14	0.10	100.1	146	97	<4	176	327	30	101
Units C-G																			
80R-2, 34-37	49.51	1.16	14.25	12.30	0.24	7.39	11.97	2.21	0.41	0.10	0.05	99.6	157	88	12	117	359	25	66
81R-2, 74-77	50.21	1.20	15.08	10.53	0.22	8.01	11.42	2.28	0.63	0.11	0.67	100.3	167	103	9	121	347	24	67
82R-2, 42-45	50.57	1.21	14.91	10.96	0.23	7.61	11.94	2.29	0.41	0.10	0.38	100.5	140	99	7	123	346	23	68
82R-2, 117-120	49.66	1.16	14.24	12.27	0.26	7.41	11.97	2.21	0.39	0.10	0.03	99.7	158	94	12	120	363	24	66
82R-4, 102-105	49.51	1.17	14.28	12.93	0.23	7.06	11.69	2.31	0.51	0.10	0.27	100.1	161	79	12	124	366	25	67
83R-1, 7-10	49.98	1.21	15.01	10.49	0.19	8.37	11.69	2.39	0.16	0.10	0.50	100.1	152	99	7	129	394	24	67
83R-2, 30-33	50.07	1.14	13.91	12.88	0.19	7.41	11.85	2.08	0.06	0.09	-0.05	99.6	120	86	<4	113	331	26	68
84R-1, 126-130	50.01	1.13	13.77	13.04	0.19	7.76	12.07	2.11	0.06	0.09	-0.02	100.2	131	86	6	111	315	24	64
84R-2, 111-115	50.48	1.14	13.95	12.94	0.19	7.55	11.77	2.05	0.06	0.10	-0.15	100.1	126	88	<4	110	321	25	67
85R-3, 16-19	49.85	1.06	13.78	12.78	0.19	7.98	11.81	2.07	0.06	0.09	0.19	99.9	173	91	5	107	321	22	60
85R-5, 112-115	50.01	1.10	13.85	12.99	0.18	7.89	11.89	2.01	0.06	0.09	0.03	100.1	152	90	<4	107	323	22	62
86R-1, 100-103	49.19	1.14	14.25	12.92	0.22	7.20	11.94	2.15	0.35	0.11	0.02	99.5	157	92	7	109	343	25	65
86R-2, 122-125	50.04	1.20	14.94	10.78	0.18	7.87	12.28	2.37	0.20	0.11	0.25	100.1	160	101	7	117	375	27	68
87R-2, 37-40	50.45	1.20	15.20	10.25	0.19	7.93	12.51	2.40	0.06	0.10	0.07	100.4	169	118	<4	115	347	27	69
87R-2, 131-135	48.79	1.15	14.46	12.63	0.21	6.92	12.02	2.25	0.57	0.10	0.32	99.4	166	89	16	113	358	23	65
87R-2, 66-70	49.35	1.17	14.21	12.99	0.27	7.12	11.83	2.28	0.54	0.10	0.19	100.1	150	84	16	118	386	23	66
88R-1, 18-21	49.28	1.13	13.89	13.27	0.22	7.35	12.19	2.14	0.12	0.10	-0.17	99.5	152	89	8	109	349	23	64
88R-1, 70-75	50.22	1.15	14.08	13.24	0.21	7.22	12.14	2.17	0.19	0.10	-0.19	100.5	154	87	5	107	339	24	65
88R-3, 18-22	50.07	1.16	14.39	12.01	0.20	7.52	12.41	2.24	0.09	0.10	-0.05	100.1	154	128	5	112	366	24	66
88R-3, 78-81	49.74	1.13	14.27	13.44	0.22	7.43	12.00	2.06	0.28	0.09	-0.24	100.4	163	87	10	107	349	24	64
89R-1, 38-42	49.44	1.17	14.10	13.05	0.22	7.73	12.28	2.08	0.03	0.10	-0.02	100.2	144	94	<4	110	346	23	67
89R-1, 110-113	50.02	1.14	14.15	11.96	0.17	7.49	12.28	2.20	0.04	0.09	-0.05	99.5	151	93	5	112	353	24	67
89R-2, 87-91	49.89	1.14	13.96	12.69	0.21	7.56	12.39	2.20	0.08	0.10	-0.29	99.9	150	88	6	108	333	23	65
89R-3, 11-15	49.64	1.11	13.79	13.31	0.20	7.38	12.19	2.11	0.18	0.10	-0.17	99.8	148	92	8	107	340	26	63
89R-3, 58-62	50.54	1.12	13.91	12.86	0.19	7.07	12.09	2.15	0.25	0.10	-0.17	100.1	155	99	10	108	347	23	64
90R-1, 21-25	49.87	1.13	13.70	12.97	0.18	7.71	12.11	2.07	0.05	0.10	0.07	100.0	145	92	5	108	339	24	64
90R-3, 72-76	49.37	1.15	14.09	12.64	0.21	7.71	12.30	2.16	0.06	0.09	-0.13	99.7	155	103	<4	107	331	24	64
91R-1, 15-18	49.17	1.14	14.06	12.75	0.23	7.75	12.48	2.33	0.07	0.10	-0.28	99.8	159	97	6	108	356	24	65
92R-1, 107-110	49.94	1.13	14.00	12.82	0.20	7.55	12.18	2.17	0.05	0.10	-0.14	100.0	163	97	5	108	351	23	64
92R-2, 100-103	50.35	1.16	14.46	12.28	0.20	7.40	12.02	2.17	0.05	0.09	-0.07	100.1	156	90	<4	110	337	26	68
93R-1, 25-28	50.17	1.15	14.24	12.72	0.21	7.45	12.15	2.13	0.15	0.10	-0.29	100.2	157	96	3	108	348	24	67
93R-1, 55-57	50.21	1.15	14.14	12.67	0.21	6.82	12.20	2.31	0.26	0.10	-0.21	99.9	163	96	10	109	343	23	65
93R-2, 59-63	50.54	1.12	13.85	12.74	0.21	6.99	11.89	2.19	0.33	0.10	-0.13	99.8	159	89	11	107	352	23	64
93R-3, 4-7	49.86	1.12	13.74	12.81	0.20	7.40	12.16	2.07	0.07	0.10	0.11	99.6	145	90	6	109	332	23	65
130-803D-																			
68R-4, 27-31	47.68	1.46	16.43	12.80	0.15	4.56	11.35	2.48	0.97	0.16	1.79	99.7	290	185	22	206	357	26	83

Table 3. Instrumental neutron activation (NNA) and inductively-coupled plasma-mass-spectrometric (ICPMS) data for Leg 130, Site 289, and Manihiki basalts.

Core, section, interval (cm)	Method	Sc	Y	Zr	Nb	Cs	Rb	Ba	La	Ce	Pr	Nd	Sm	Eu	Gd	Tb	Dy	Ho	Er	Yb	Lu	Hf	Ta	Th	U	
130-807C-																										
Unit A																										
74R-1, 46-49	NAA	48							4.7	10.6		7.7	3.2	1.1	3.6	0.7				2.3	0.31	2.18	0.28	0.39		
74R-2, 118-122	ICPMS	42	31	101	6.2	0.04	5	24	6.1	15.0	2.3	11.2		1.3	4.5		4.9	1.1	2.9	2.8	0.42	2.64	0.44	0.45	0.13	
75R-1, 27-30	ICPMS	50	28	93	5.6	0.77	33	24	5.3	13.2	2.0	10.0	3.0	1.2	3.8		4.2	0.9	2.6	2.4	0.33	2.25	0.35	0.46	0.16	
75R-2, 125-129	ICPMS	50	32	102	5.8	0.01	3	17	5.8	14.9	2.3	11.2	3.3	1.3	4.7		5.3	1.2	3.3	3.0	0.50	2.72	0.45	0.58	0.14	
75R-4, 48-52	NAA	46							6.2	14.6		11.7	3.4	1.3	4.5	0.8				2.7	0.42	2.64	0.34	0.56		
77R-1, 48-51	NAA	43							6.0	14.4		11.4	3.5	1.4	4.6	0.8				2.7	0.42	2.64	0.35	0.56		
78R-1, 63-67	ICPMS	44	31	102	5.8	0.03	4	30	5.8	15.2	2.3	11.1	3.5	1.4	4.5		5.3	1.2	3.4	3.0	0.43	2.75	0.41	0.62	0.15	
79R-3, 110-114	ICPMS	46	29	97	6.1	0.21	10	25	6.0	15.4	2.4	11.5	3.5	1.3	4.3	0.8	5.0	1.0	2.8	2.8	0.43	2.54	0.36	0.51	0.12	
79R-4, 25-28	ICPMS	44	29	93	5.6	0.28	12	27	6.3	15.8	2.4	11.6	3.6	1.3	4.3		5.0	1.0	3.0	2.7		2.50	0.40	0.54	0.13	
79R-5, 34-38	ICPMS	52	31	100	6.1	0.01	3	22	5.7	14.8	2.3	10.5	3.2	1.3	4.3		4.9	1.0	2.9	2.8		2.49	0.38	0.56	0.14	
Units C-G																										
80R-2, 34-37	ICPMS	47	26	66	3.7	0.15	10	10	3.4	9.4	1.5	7.5	2.5	0.9	3.3		4.2	0.9	2.6	2.6		1.73	0.22	0.30	0.08	
83R-1, 7-10	ICPMS	61	24	63	3.5	0.01	4	14	3.2	9.1	1.4	7.1	2.4	0.9	3.3		3.8	0.9	2.2	2.2	0.34	1.57	0.21	0.26	0.21	
	NAA	51							3.3	9.6		8.1	2.6	1.0	3.5	0.7				2.4	0.38	1.81	0.21	0.35		
86R-2, 122-125	ICPMS	52	28	68	3.5	0.02	4	11	4.0	10.4	1.7	7.9	2.6	1.0	3.6		4.8	1.0	2.8	2.8		1.89	0.24	0.27	0.18	
88R-3, 18-22	ICPMS	50	26	65	3.5	0.02	5	10	3.6	9.5		7.5	2.4	1.0	3.2		4.2	0.9	2.6	2.4		1.67	0.24	0.28	0.08	
88R-3, 78-81	NAA	52							3.0	8.1		6.5	2.3	0.9	3.4	0.7				2.4	0.38	1.74	0.20	0.34		
89R-2, 87-91	ICPMS	58	24	66	3.7	0.10	5	13	3.0	7.8	1.3	6.2		0.9	2.9		3.5	0.8	2.1	2.1		1.50	0.21	0.26	0.18	
90R-1, 21-25	ICPMS	47	25	63	3.4	0.01	2	17	3.4	8.7	1.4	7.0	2.5	0.9	3.3	0.6	3.9	0.9	2.4	2.3	0.35	1.66	0.20	0.23	0.09	
	ICPMS	41	25	63	3.5	0.01	2	17	3.5	9.0	1.4	7.0	2.4	0.9	3.3	0.6	3.9	0.9	2.4	2.5		1.79	0.22	0.28	0.10	
92R-1, 107-110	ICPMS	49	24	63	3.5	0.01	4	17	3.6	9.1	1.5	7.4	2.3	0.9	3.2		4.1	0.9	2.5	2.4		1.79	0.22	0.28	0.08	
	NAA	48							3.6	8.0		7.0	2.3	0.9	3.1	0.6				2.3	0.36	1.70	0.19	0.31		
93R-3, 4-7	ICPMS	52	24	62	3.3	0.01	4	17	3.2	9.8	1.4	6.8	2.1	0.9	3.1		4.0	0.9	2.5	2.4	0.33	1.69	0.19	0.29	0.08	
	NAA	46							3.4	7.6		6.8	2.1	0.9	3.0	0.6				2.3	0.36	1.70	0.19	0.31		
130-803D-																										
68R-4, 27-31	NAA	48							4.7	10.6		7.7	3.2	1.1	3.6	0.7				2.3	0.31	2.18	0.28	0.39		
69R-1, 10-12	ICPMS	53	26	76	4.5	0.13	8	11	4.0	10.7		8.6	2.7	1.1	3.5		4.2	0.9	2.5	2.4		1.94	0.30	0.33	0.14	
69R-2, 130-133	ICPMS	53	26	79	4.1	0.09	8	13	3.8	10.1	1.7	8.3	2.7	1.1	3.8	0.7	4.7	1.0	2.8	2.7	0.37	2.04	0.31	0.33	0.35	
69R-4, 29-31	ICPMS	54	36	86	4.7		23	36	5.7	12.3	2.1	9.9		1.2	4.1		5.0	1.1	3.1	3.0		2.28	0.33	0.37	0.34	
	NAA	49							5.6	11.7		10.0	3.0	1.3	4.1	0.8				2.9	0.48	2.33	0.28	0.41		
70R-3, 25-29	ICPMS	43	27	82	5.1	0.27	15	20	4.1	10.6	1.7	8.5		1.1	3.7		4.2	0.9		2.6	0.37	2.01	0.31	0.33	0.22	
71R-1, 125-127	ICPMS	44	26	76	4.3	0.10	10	9	4.1	10.4	1.7	8.2		1.1	3.6		4.1	0.9	2.5	2.5		1.92	0.29	0.36	0.09	
71R-2, 134-137	ICPMS	47	26	74	4.0	0.31	9	10	3.8	10.2	1.7	8.0	2.8	1.1	3.8		4.5	1.0	2.8	2.6	0.39	2.14	0.29	0.33	0.10	
	NAA	49							4.3	10.2		7.9	2.7	1.0	3.6	0.7				2.3	0.36	1.96	0.25	0.36		
130-289-																										
132-3, 52-55	NAA	46							4.3	11.7		9.9	3.3	1.2	4.4	0.8				3.1	0.48	2.46	0.45			
Manihiki Plateau																										
33-317A-																										
31-4, 116-118	NAA	38							2.6	7.5		6.3	1.9	0.8	3.0					2.1	0.32	1.50	0.35			
34-4, 83-85	NAA	45							4.4	10.8		9.1	2.7	1.1	3.7	0.6				2.5	0.38	2.08	0.52			
Standards:																										
BOB-1 Meas.	NAA	33	—	—	—	—	—	—	4.8	12.4	—	9.9	3.0	1.2	3.8	0.8	—	—	—	2.6	0.39	2.43	0.43	0.40	—	—
BOB-1 Rec.		—	—	—	—	—	—	—	4.7	13.8	—	10.7	3.3	1.3	—	0.7	—	—	—	2.6	0.44	2.53	0.51	0.45	—	—
W-2 Meas.	ICPMS	36	22	94	7.9	0.96	21	171	10.9	23.4	3.1	13.1	3.3	1.1	3.8	0.6	3.7	0.8	2.1	2.0	0.30	2.35	0.53	2.37	0.52	
W-2 Rec.		35	24	102	8.0	1.03	21	172	10.6	22.6	3.2	15.1	3.5	1.2	4.2	0.6	4.3	0.8	2.4	2.1	0.36	2.62	0.50	2.57	0.54	

Notes: All abundances are in ppm. For NAA data, precision was determined from eight replicate analyses of Standard BOB-1, except for Sc, for which six replicates were analyzed. Precisions, as estimated by standard deviations (in ppm), are: Sc = 1.4, La = 0.08, Ce = 0.32, Nd = 0.26, Sm = 0.10, Eu = 0.03, Tb = 0.07, Yb = 0.08, Lu = 0.01, Hf = 0.07, Ta = 0.01, and Th = 0.02. A measure of NAA accuracy is provided by recommended vs. our average measured values for BOB-1, and of ICPMS accuracy by the average of six recent analyses of W-2 vs. Jenner et al.'s [1990] preferred values. The standard deviations of the W-2 analyses are (in ppm): Sc = 1.7, Y = 1.3, Zr = 4.5, Nb = 0.2, Cs = 0.08, Rb = 0.9, Ba = 7.0, La = 0.48, Ce = 0.76, Pr = 0.16, Nd = 0.59, Sm = 0.17, Eu = 0.05, Gd = 0.13, Tb = 0.05, Dy = 0.17, Ho = 0.05, Er = 0.07, Tm = 0.03, Yb = 0.06, Lu = 0.03, Hf = 0.13, Ta = 0.06, Th = 0.18, and U = 0.02.

following methods described by Mahoney and Spencer (1991) and Mahoney et al. (1991). These methods included, before grinding, the ultrasonic cleaning of handpicked, interior rock chips (~3 mm across) in ultra-pure, weak HNO<sub>3</sub>-HF, 6N HCl, and H<sub>2</sub>O (in sequence) to remove possible surface Pb contamination. In one case, we picked fresh, crystal-free glass from a flow margin (Unit A, Sample 130-807C-77R-2, 108–110 cm). Note that the selective picking of fresher appearing chips or crystal-free glass from the bulk sample, and the subsequent cleaning procedure, often mean that the portion of the sample analyzed for isotopes does not faithfully represent the whole rock *chemically*; therefore, the isotope-dilution abundance measurements in Tables 4 and 5 should not, in general, be compared directly with the whole-rock chemical data in Tables 2 and 3. As an illustration, isotope-dilution values for two bulk samples (~2 cm across, interior pieces) that were not picked and were cleaned only in ultra-pure water are given in Tables 4 and 5 ("UP" Samples 130-803D-71R-1, 124–126 cm, and 130-807C-79R-5, 38–40 cm) together with the respective analyses for their picked and cleaned chips. As expected, the bulk-sample results for Nd, Sm, and Sr are within about 10% of the corresponding X-ray fluorescence or inductively coupled plasma-mass-spectrometric values in Tables 2 and 3, but they show significant differences from those for the picked and cleaned chips. Tables 4 and 5 also list our isotopic and isotope-dilution analyses of the USGS standard rock BCR-1.

In addition to the above measurements, Sr isotopes were determined on severely acid-leached splits of powder. For moderately to rather highly altered tholeiitic samples, the leaching procedure used

largely removes the effects of low-temperature seawater alteration on <sup>87</sup>Sr/<sup>86</sup>Sr by producing a residue of relatively fresh material, mainly clinopyroxene, plagioclase, and, if present, fresh glass (Mahoney, 1987). Comparison of the calculated initial (<sup>87</sup>Sr/<sup>86</sup>Sr)<sub>T</sub> values of the two leached Site 807 Unit A powders with that of the fresh glass, for example, shows no significant differences. In the illustrations and in the discussion that follows, we use the Sr isotopic values for the leached aliquants. Unlike Sr isotopes, Nd isotopic ratios appear not to be affected significantly by levels of alteration greater than those suffered by the Leg 130 samples chosen for isotopes (Mahoney, 1987; Cheng et al., 1987; Staudigel et al., 1991; Castillo et al., 1991). Likewise, Pb isotopic ratios of unleached and acid-leached pairs previously were found to be very similar for moderately altered tholeiites from the Manihiki Plateau, and for the more highly altered Ontong Java basalt from Site 289 (Mahoney and Spencer, 1991). In Table 5, the Pb isotope values for the fresh glass and the two unleached samples from Unit A are identical within errors.

## Results

All of the samples analyzed are quartz- or olivine-normative tholeiitic basalts, broadly similar in chemical composition to the flow at DSDP Site 289 (see Table 3), to basement lavas on the island of Malaita (Spencer et al., unpubl. data, 1991), as well as to the Early Cretaceous flows and sills filling the Nauru Basin (e.g., Floyd, 1986; Saunders, 1986; Castillo et al., 1986, 1991), which borders the plateau on the east and probably is genetically related to it (e.g., Tokuyama

**Table 4. Nd and Sr isotopic and isotope-dilution data for Leg 130 basalts.**

Core, section, interval (cm)		( <sup>143</sup> Nd/ <sup>144</sup> Nd) <sub>0</sub>	( <sup>87</sup> Sr/ <sup>86</sup> Sr) <sub>0</sub>	Nd(ppm)	Sm	Sr	Rb	( <sup>87</sup> Sr/ <sup>86</sup> Sr) <sub>T</sub>	( <sup>143</sup> Nd/ <sup>144</sup> Nd) <sub>T</sub>	ε <sub>Nd</sub> (T)
130-803D- 69R-2, 54–56	UL	0.512944	0.70472	8.225	2.710	137.9	14.0	0.70434	0.512827	+5.9
	L		0.70391							
71R-1, 124–126	UP	0.512944	0.70439	8.616	2.800	145.6	3.61	0.70430	0.512828	+5.9
	UL	0.512950	0.70389	4.862	1.823	130.5	2.07	0.70383	0.512917	+5.7
	L		0.70369			109.3	1.33	0.70364		
130-807C- 75R-4, 46–48 Unit A	UL	0.512897	0.70438	9.331	3.031	166.2	1.60	0.70433	0.512743	+5.0
	L		0.70408							
77R-2, 108–110 Unit A	GL	0.612878	0.70417	10.98	3.370	148.9	3.53	0.70405	0.512732	+4.8
79R-5, 38–40 Unit A	UP	0.612913	0.70444	11.53	3.552	170.0	1.12	0.70441	0.612767	+5.5
	UL	0.512926	0.70426	7.582	2.587	165.8	0.964	0.70423	0.512764	+5.4
	L		0.70413			159.8	0.951	0.70410		
82R-2, 121–123 Unit C	UL	0.512966	0.70383	6.336	1.932	105.8	4.37	0.70363	0.512793	+6.0
	L		0.70356				85.66	2.11		
82R-4, 105–107 Unit E	UL	0.5129U	0.70407	6.255	2.158	106.2	6.13	0.70378	0.512800	+6.1
	L		0.70367				80.53	4.08		
85R-3, 19–21 Unit F	UL	0.512983	0.70357	3.594	1.314	97.55	0.743	0.70354	0.512810	+6.3
	L		0.70347				68.22	0.211		
88R-3, 76–79 Unit G	UL	0.512965	0.70377	5.142	1.891	93.53	4.97	0.70366	0.512790	+5.9
	L		0.70358				100.1	3.81		
USGS Standard BCR-1		0.512633	0.70502	28.51	6.576	329.4	46.2			

Notes: T = 120 Ma for Site 807, 90 Ma for Site 803. UL = unleached, but chips handpicked and acid-cleaned; L = strongly acid-leached powder; UP = bulk sample, not picked, cleaned only in H<sub>2</sub>O. GL = handpicked, fresh glass. Isotopic fractionation corrections are <sup>148</sup>Nd/<sup>144</sup>Nd = 0.242436 (<sup>148</sup>Nd/<sup>144</sup>Nd = 0.291572), <sup>86</sup>Sr/<sup>88</sup>Sr = 0.1194. Data are reported relative to University of Hawaii standard values: for La Jolla Nd, <sup>143</sup>Nd/<sup>144</sup>Nd = 0.511855; for BCR-1, see above; for NBS 987 Sr, <sup>87</sup>Sr/<sup>86</sup>Sr = 0.71025; for E and A Sr, <sup>87</sup>Sr/<sup>86</sup>Sr = 0.70803. The total range measured for La Jolla Nd is ±0.000012 (0.2ε units); for NBS 987 it is ±0.000022. Within-run errors on the isotopic data above are less than or equal to the external uncertainties on these standards. Total blanks are negligible: <20 picograms for Nd and <120 picograms for Sr. Uncertainties on Nd and Sm abundances are estimated at <0.2%; on Sr and Rb, <0.5% and ~1%, respectively. ε<sub>Nd</sub>(T) = 0 today corresponds to <sup>143</sup>Nd/<sup>144</sup>Nd = 0.512640; ε<sub>Nd</sub>(T) = 0 at 120 Ma corresponds to (<sup>143</sup>Nd/<sup>144</sup>Nd)<sub>T</sub> = 0.512486 for <sup>147</sup>Sm/<sup>144</sup>Nd = 0.1967, and to 0.512524 at 90 Ma.

Table 5. Pb isotopic and isotope-dilution data for Leg 130 basalts.

Core, section, interval (cm)	$^{206}\text{Pb}/^{204}\text{Pb}$	$^{207}\text{Pb}/^{204}\text{Pb}$	$^{208}\text{Pb}/^{204}\text{Pb}$	Pb (ppm)
130-803D-69R-2, 54–56	18.691	15.529	38.448	0.368
71R-1, 124–126	18.626	15.522	38.426	0.255
UP	18.643	15.523	38.436	0.363
130-807C-75R-4, 46–48	18.395	15.531	38.383	0.581
Unit A				
77R-2, 108–110	18.392	15.533	38.398	0.562
Unit A				
79R-5, 38–40	18.385	15.521	38.368	0.505
Unit A	18.392	15.526	38.387	0.659
82R-2, 121–123	18.635	15.523	38.455	0.295
Unit C				
82R-4, 105–107	18.659	15.489	38.402	0.227
Unit E				
85R-3, 19–21	18.609	15.522	38.391	0.278
Unit F				
88R-3, 76–79	18.668	15.547	38.535	0.270
Unit G				
USGS Standard BCR-1	18.805	15.619	38.669	13.53

Notes: UP = bulk sample, not picked, cleaned only in H<sub>2</sub>O. Chips of other samples were handpicked and acid-cleaned in HF-HN<sub>3</sub> and HCl. GL = handpicked fresh glass. Pb isotopic ratios are present-day values, corrected for fractionation using the NBS 981 standard values of Todt et al. (1984); the total ranges measured for NBS 981 are +0.008 for  $^{206}\text{Pb}/^{204}\text{Pb}$ ,  $\pm 0.008$  for  $^{207}\text{Pb}/^{204}\text{Pb}$ , and  $\pm 0.030$  for  $^{208}\text{Pb}/^{204}\text{Pb}$ . Within-run uncertainties ( $2\sigma_m$ ) on the isotopic data above are generally less than these values, and in all cases less than  $\pm 0.012$ ,  $\pm 0.012$ , and  $\pm 0.038$ . Estimated uncertainty on Pb abundances is <1%. Total procedural blanks are negligible at 5–30 picograms.

and Batiza, 1981; Castillo et al., 1991). As with the Site 289, Malaitan, and Nauru Basin basalts, both the major and many trace element abundances of the Leg 130 lavas overlap the range of values for mid-ocean-ridge basalts (MORB). For example, TiO<sub>2</sub> (1.06–1.70 wt%), P<sub>2</sub>O<sub>5</sub> (generally 0.09–0.20 wt%), Zr (60–102 ppm), and the rare-earth elements have values typical of normal MORB. Ba (9.4–36 ppm), Th (0.31–0.56 ppm), Ta (0.19–0.37 ppm), Nb (3.4–6.2 ppm), Sr (107–250 ppm), and, in the fresher samples, K<sub>2</sub>O (<0.2 wt%) also overlap the MORB range but exceed average values for normal MORB (approximately 6.3, 0.12, 0.13, 2.3, and 90 ppm, and 0.07 wt%, respectively; e.g., Sun and McDonough, 1989). However, their upper limits still lie well within the range of values found at spreading centers, among so-called “transitional” or “enriched” MORB. Compared with normal MORB, all of the Leg 130 rocks display slight enrichments in highly incompatible elements relative to moderately incompatible elements (e.g., Zr/Nb = 16–19 vs. >30 for normal MORB [e.g., Sun and McDonough, 1989]; also see Fig. 6); the same is true of the Site 289, Malaitan, and Nauru Basin lavas and, indeed, is a feature common to the small number of basaltic samples available from the other Pacific plateaus (Floyd, 1986; Saunders, 1986; Mahoney, 1987).

### Isotopes

Figures 7 and 8 show that, isotopically, the Leg 130 basalts are very similar to the few samples measured previously from DSDP Site 289 and southern Malaita (Mahoney and Spencer, 1991). Total variation in initial  $\epsilon_{\text{Nd}}(T)$  is +4.8 to +6.3 for the Leg 130 lavas; initial  $(^{87}\text{Sr}/^{86}\text{Sr})_T$  lies between 0.70339–0.70410 for acid-leached powders and glass. As expected, unleached powders have greater (as much as 0.0006 greater) and more variable Sr-isotope ratios, depending on their level of alteration. Present-day  $^{206}\text{Pb}/^{204}\text{Pb}$  is between 18.385 and 18.691,  $^{207}\text{Pb}/^{204}\text{Pb}$

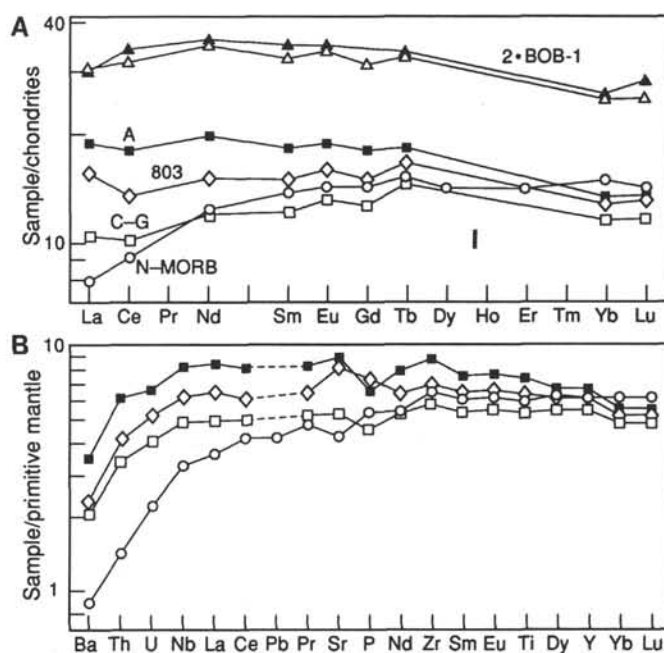


Figure 6. **A.** Average chondrite-normalized rare-earth-element patterns for Site 803 (open diamonds), Site 807 Unit A (filled squares), and Units C–G (open squares). All of the Leg 130 basalts are enriched slightly in the light rare earths relative to normal MORB (represented by open circles). Also shown are measured (open triangles) and recommended (filled triangles) values for standard BOB-1 (plotted as twice the true values for clarity). Normalizing values are those of Hanson (1980). **B.** Average primitive-mantle-normalized element patterns; normalizing values are those of Sun and McDonough (1989). U values for several Site 803 and Units C–G samples were not included in the average because these samples are comparatively highly altered (e.g., their Th/U <2).

= 15.489 to 15.547, and  $^{208}\text{Pb}/^{204}\text{Pb}$  = 38.368 to 38.535. An estimate of the range of initial Pb isotopic ratios is provided by bulk-sample U/Pb and Th/Pb for Samples 130-803D-71R-1, 124–127 cm ( $^{238}\text{U}/^{204}\text{Pb}$  = 16 and  $^{232}\text{Th}/^{204}\text{Pb}$  = 65) and 130-807C-79R-5, 34–40 cm ( $^{238}\text{U}/^{204}\text{Pb}$  = 14 and  $^{232}\text{Th}/^{204}\text{Pb}$  = 56). Assuming U has not been elevated appreciably by alteration in these two samples (as implied by their relatively high, oceanic-island-like Th/U values of 4.0), these ratios are 18.13–18.42, 15.51–15.51, and 38.04–38.15.

Although the total range of isotopic variation is rather limited, the Leg 130 data can be seen to cluster into two groups on Figure 8. The Unit A flows have lower  $^{206}\text{Pb}/^{204}\text{Pb}$  (18.385–18.395), higher  $(^{87}\text{Sr}/^{86}\text{Sr})_T$  (0.70403–0.70410), and lower  $\epsilon_{\text{Nd}}(T)$  (+4.8 to +5.4) than those of Units C–G (18.609–18.668, 0.70339–0.70345, +5.9 to +6.3, respectively). The Site 803 samples are like those of Units C–G in Pb isotopes (18.626–18.691), with slightly greater  $(^{87}\text{Sr}/^{86}\text{Sr})_T$  and lower  $\epsilon_{\text{Nd}}(T)$  (0.70364–0.70373, +5.7 to +5.9, respectively). In comparison, the Site 289 flow (18.708, 0.70346, +6.3) is virtually identical to the Unit C–G lavas, whereas the basalts from southern Malaita (18.245–18.521, 0.70404–0.70423, +4.0 to +4.9) closely resemble the Unit A flows. These results require the existence of subtly different mantle sources among the plateau lavas sampled to date. Note also that a recent suggestion that Malaita may not be part of the plateau but an unrelated piece of the Australian Plate (Musgrave, 1990) is not supported by either the strong isotopic resemblance of the Malaitan samples to the Unit A flows, their very similar chemical characteristics (Spencer et al., unpubl. data, 1991), or  $^{40}\text{Ar}$ – $^{39}\text{Ar}$  dates of 122–123 Ma for Malaitan basement (R.A. Duncan, unpubl. data, 1991), which are identical to those for Sites 807 and 289. In the subsequent discussion, therefore, we include the Malaitan data with results for the drillholes.

The combined Ontong Java measurements fall within the overall field of oceanic-mantle-derived rocks but lie outside the specific

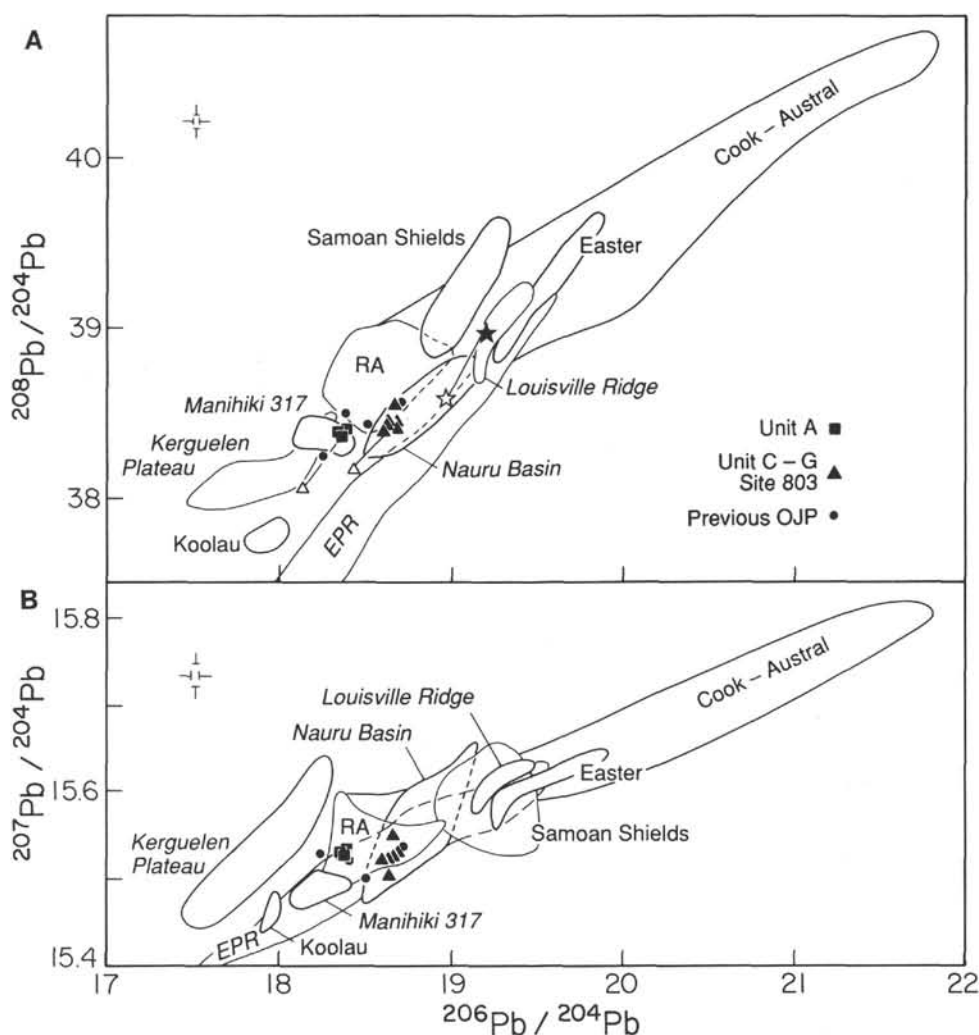


Figure 7. Present-day  $^{208}\text{Pb}/^{204}\text{Pb}$  vs.  $^{206}\text{Pb}/^{204}\text{Pb}$  (A) and  $^{207}\text{Pb}/^{204}\text{Pb}$  vs.  $^{206}\text{Pb}/^{204}\text{Pb}$  (B) for Leg 130, Site 289, and southern Malaitan basalts. Triangles indicate Site 807 Units C-G and Site 803 data; squares are for Site 807 Unit A; circles are for Site 289 and Malaitan lavas (= Previous OJP; Mahoney and Spencer, 1991). Open triangles represent initial Pb isotopic ratios estimated from U, Th, and Pb abundances for bulk samples 130-803D-71R-1, 124-127 cm, and 130-807C-79R-5, 34-40 cm. Solid and open stars in Figure 7A illustrate the estimated 120-m.y. change in Pb isotopes for the mantle source of a typical Louisville Ridge basalt (SOTW 58-1; calculated using isotopic ratios of Cheng et al. [1987], measured U and Th, and estimated Pb (assuming Ce/Pb = 25) abundances from Hawkins et al. [1987]). Note that this is a probable maximum change as the Th/Pb and U/Pb values for the source are likely to be lower than in these alkalic basalts. Fields for the Kerguelen Plateau (Weis et al., 1989; Storey et al., 1992) and the Manihiki Plateau at DSDP Site 317 (Mahoney and Spencer, 1991) are also shown, along with ones for East Pacific Rise MORB (EPR) (White et al., 1987; Hanan and Schilling, 1989; Prinzhofer et al., 1989; Mahoney et al., unpubl. data, 1991), Nauru Basin, Louisville Ridge, and selected Pacific oceanic islands (see references of Mahoney and Spencer, 1991). RA = Rarotonga. Error bars are for data reported in this paper.

fields of Pacific MORB and the majority of present-day Pacific oceanic islands, the latter being characterized by greater  $^{206}\text{Pb}/^{204}\text{Pb}$ . Rarotonga, Pitcairn, and several Hawaiian shields (e.g., Koolau) are exceptions, but they are all located very far away from the estimated 120-Ma position of the plateau. The Ontong Java isotopic data also are unlike those of many continental tholeiites, which often fall well outside the oceanic mantle field (e.g., Hawkesworth et al., 1990). In addition, the elemental ratios Nb/Th (11-16 for our samples) and Nb/U (37-51 for the less altered samples) are sensitive indicators of continental crustal contamination, as crustal values tend to be much lower than oceanic mantle ones (e.g., Hofmann et al., 1986); the Leg 130 data, however, are firmly within the oceanic mantle range. Thus, no geochemical evidence exists of a continental basement to the plateau,

as suggested by some earlier workers on geophysical grounds (see discussion and references of Mahoney and Spencer, 1991).

Although the four basement sites now sampled are perhaps unlikely to be truly representative of an edifice as extensive as the Ontong Java Plateau, the entire range of isotopic variation observed at these widely separated locations is quite small. Indeed, their relative uniformity is emphasized by comparison to the Manihiki and Kerguelen plateaus. Basement lavas have been sampled at only two locations on the Manihiki Plateau: (1) DSDP Site 317 (with 33.5 m of basement penetration) and (2) a dredge haul ~300 km to the northwest (data for the latter are not included on Figs. 7 or 8); yet they show a significantly greater spread of isotopic variation than the Ontong Java rocks ( $^{206}\text{Pb}/^{204}\text{Pb}$  varies from 18.10 to 19.35, and  $\epsilon_{\text{Nd}}(\text{T})$  from +0.8 to +6.8;

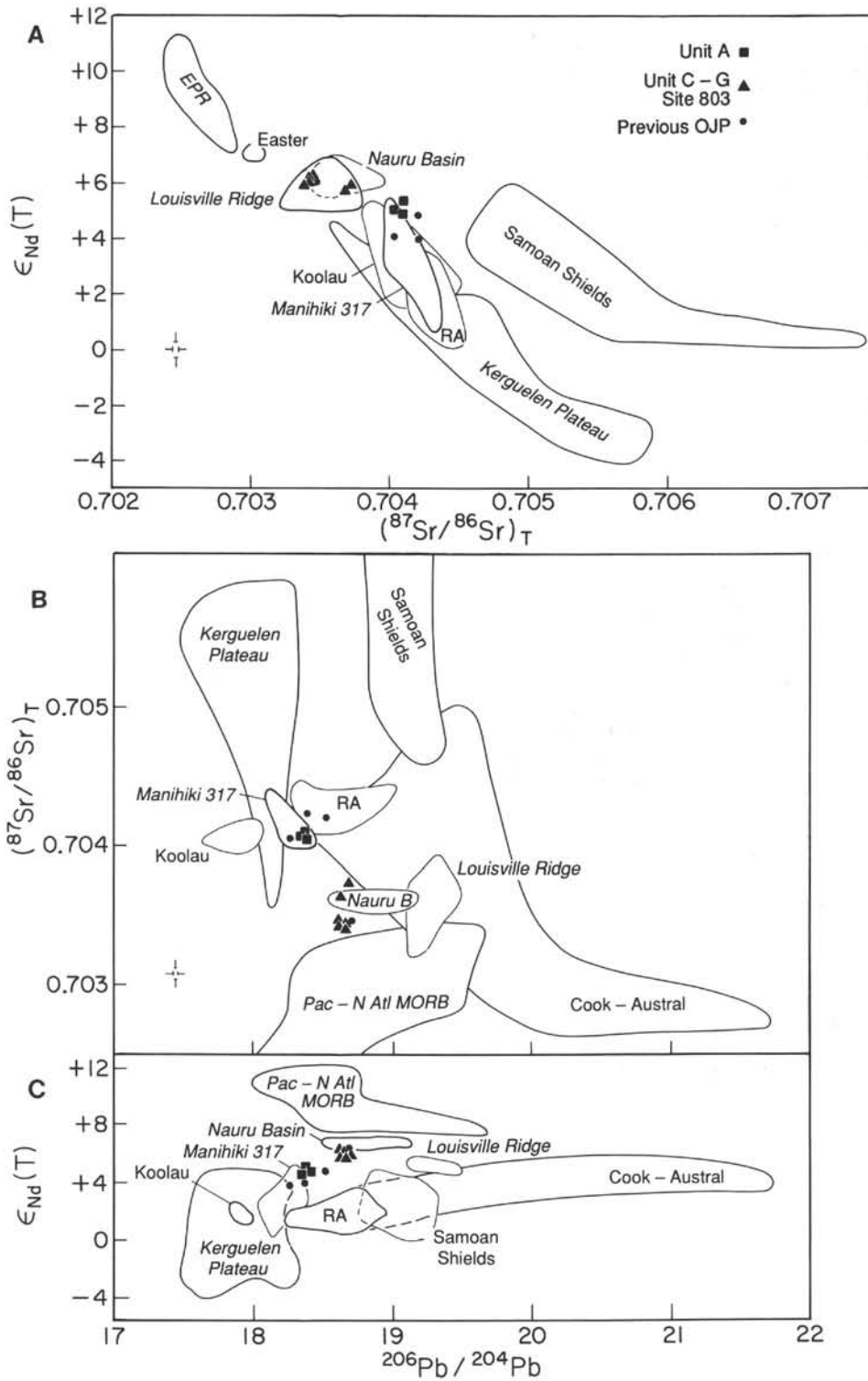


Figure 8.  $\epsilon_{Nd}(T)$  vs.  $(^{87}Sr/^{86}Sr)_T$  (A),  $(^{87}Sr/^{86}Sr)_T$  vs.  $^{206}Pb/^{204}Pb$  (B), and  $\epsilon_{Nd}(T)$  vs.  $^{206}Pb/^{204}Pb$  (C) for Leg 130, Site 289, and Malaitan basalts. Symbols are as in Figure 7; data sources are as in Figure 7 (this study) and in Figure 3 of Mahoney and Spencer (1991). Error bars are for results reported in this paper.

Mahoney and Spencer, 1991). Basalts from several dredges and drillholes on the Kerguelen Plateau cover an extreme range of  $\epsilon_{Nd}(T)$  (+5.2 to -4) and possess variable—and low— $^{206}Pb/^{204}Pb$  (17.47–18.28) as well (Weis et al., 1989; Storey et al., 1992; Salters et al., 1992). Despite their differences, all three plateau data sets are characterized by a combination of high  $^{208}Pb/^{204}Pb$  and low  $\epsilon_{Nd}(T)$  for a given  $^{206}Pb/^{204}Pb$  value in comparison to Pacific MORB. This feature imparts a distinctive “DUPAL”-like (e.g., Hart, 1988) isotopic signature to all.

### Trace and Major Elements

Trace element differences also are evident between Units A and C–G, with Unit A lavas having higher abundances of (alteration-resistant) incompatible elements and small relative enrichments in highly incompatible elements compared with moderately incompatible ones. The chondrite-normalized rare-earth-element patterns (Fig. 6) of Unit A lavas, for example, show slight enrichment in the light rare earths, whereas Units C–G have lower overall abundances of rare-earth elements and flat to slightly light-rare-earth-depleted patterns. Patterns of Site 803 samples are similar in shape to those of the Site 807 rocks, with abundances intermediate between Units A and C–G. The isotopic differences noted above between Units A and C–G suggest that differences in mantle source composition are partly responsible for their respective incompatible element characteristics. Nonetheless, just as with isotopes, the overall range of incompatible element variation for the Leg 130 rocks is small. Cretaceous basement samples from the Kerguelen Plateau show much greater variability and are significantly more enriched in highly incompatible elements such as Th and Ba (i.e., they are much less MORB-like; see Fig. 9). Few comprehensive trace element analyses of good quality are available for the Manihiki Plateau; but as Figure 9 illustrates, the two Site 317 samples measured in this study have slightly higher Th/Ta and Ba/Ta than most of the Ontong Java lavas. Their normalized rare-earth-element patterns are flat, however, much like those of the Ontong Java rocks. Significantly, despite their DUPAL-like isotopic signatures, neither the Ontong Java nor the Manihiki Site 317 basalts have the high Ba/Ta (or Ba/Nb) values so characteristic of South Atlantic and Indian Ocean DUPAL-type plateaus or islands (see Fig. 9A).

Major element compositions of the Site 807 basalts reflect variable but rather high amounts of fractionation: MgO ranges from 6.1 to 8.4 wt% (excluding the uppermost, highly altered sample at the top of basement), whereas total Fe as  $Fe_2O_3$  (=  $Fe_2O_3^*$ ) is elevated, varying from 10.3 to 14.9 wt%. Site 803 lavas have slightly lower MgO (most samples are 5.3–7.5 wt%) but also lower  $Fe_2O_3^*$  (9.8–13.3 wt%) and higher Cr (236–296 vs. 126–173 ppm for Site 807) and Ni (83–185 vs. 72–126 ppm), suggesting that some are less evolved than the Site 807 flows. Also, they have higher  $Al_2O_3$  and lower  $CaO/Al_2O_3$ . Figure 10 displays major element variations for the Leg 130 basalts. Interestingly, the Site 807 data again fall into two clusters corresponding to Units A and C–G, the Unit A lavas being characterized by lower MgO and  $SiO_2$ , and greater  $TiO_2$  and  $Na_2O$  than Units C–G. Predicted 1-atm liquid evolution paths, determined by the method of Weaver and Langmuir (1990), are depicted for 25% fractional crystallization from two high-MgO samples that bracket the range of Na, Ca, Al, and Fe oxide values. These trajectories illustrate that Unit A and Units C–G cannot be related to a common parental liquid composition by low-pressure differentiation (see the diagram for  $SiO_2$ , in particular). At pressures greater than 8–10 kb, plagioclase is not stable and the fractionating phase assemblage would consist of clinopyroxene and orthopyroxene (e.g., Bender et al., 1978). Under such conditions, FeO and  $Al_2O_3$  should both increase, and  $CaO/Al_2O_3$  decrease, with progressive fractionation, but this is contrary to what is observed. Several Site 807 samples from Units C–G do have lower FeO (and higher MgO) than the Unit A basalts, but they also have higher  $Al_2O_3$ . Thus, the major element results appear to require somewhat different parental liquids for

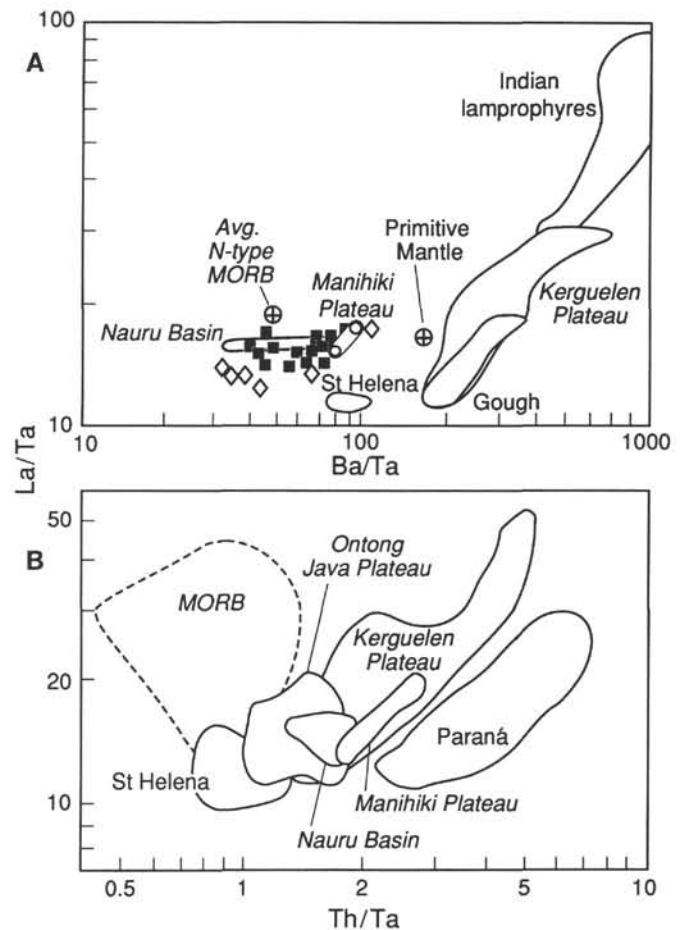


Figure 9. A. Plot of Ba/Ta vs. La/Ta, illustrating that the Pacific plateaus (as represented by the Ontong Java and Manihiki Site 317 data) are quite distinct from the Kerguelen Plateau and so-called DUPAL oceanic islands (such as Gough) or high  $^{206}Pb/^{204}Pb$  islands (such as St. Helena). Filled squares = Site 807, diamonds = Site 803, and circles = Site 317. A field for Cretaceous Indian lamprophyres (thought to have originated in the Gondwanan lithospheric mantle) illustrates the possible role of Gondwanan lithosphere in the formation of the Kerguelen Plateau. Data sources: primitive mantle and average N-type MORB, Sun and McDonough (1989); St. Helena, Chaffey et al. (1989); Gough, Weaver, et al. (1987); Nauru Basin, Saunders (1986); Kerguelen Plateau, Storey et al. (1992) and Mehl et al. (1991); Indian lamprophyres, Paul and Potts (1981). B. Th/Ta vs. La/Ta. Note that the Ontong Java basalts have more MORB-like Th/Ta than those for either the Kerguelen or Manihiki plateaus, whereas the Paraná continental flood basalts of Brazil (ca. 130 Ma) possess even greater Th/Ta values than the Kerguelen Plateau.

Unit A than for Units C–G. Similar reasoning suggests the same is true for Site 803.

## DISCUSSION

### Melting Conditions of Plateau Magmas

A major unanswered question about oceanic plateaus in general concerns the conditions of melting under which plateau lavas were generated. Figure 11 shows average  $Na_8$  vs. average  $Fe_8$  for Units A and C–G (i.e., the average fractionation-corrected  $Na_2O$  and total Fe as FeO backtracked to 8 wt% MgO; Klein and Langmuir, 1987), along with regional averages for portions of several present-day oceanic ridges. The Site 807 data lie on the trend of MORB regional averages defined by Klein and Langmuir's (1987, 1989) worldwide compilation for spreading centers; moreover, the values for each group of

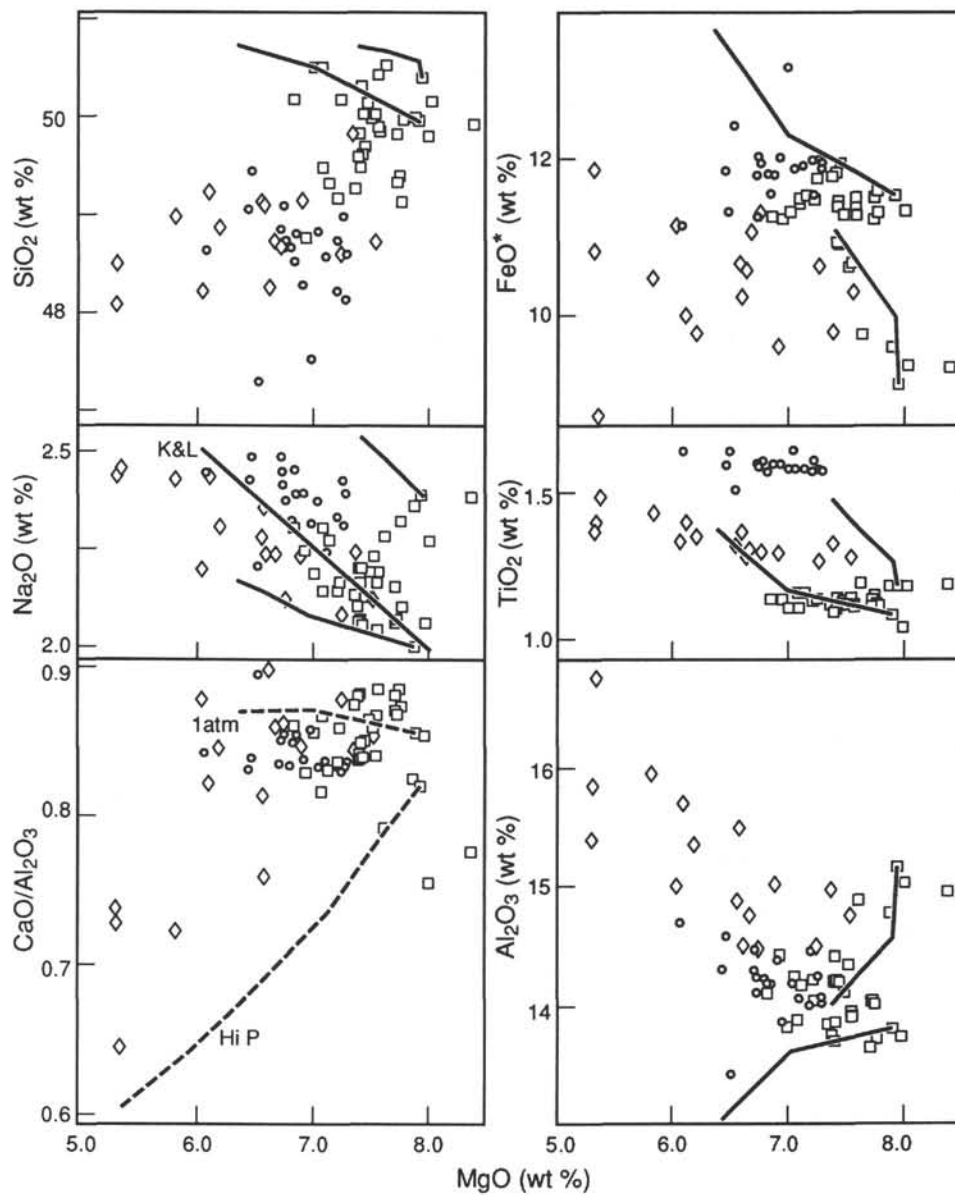


Figure 10. Major element variations vs. MgO for the Site 807 (Unit A = circles, Units C–G = squares) and Site 803 (diamonds) samples. Also shown are two trajectories representing 0%–25% low-pressure fractional crystallization calculated using the procedure of Weaver and Langmuir (1990). The two starting compositions for these paths were chosen because they span the ranges in most oxides (at high MgO) found in our samples. One low-pressure (dashed line, labeled 1 atm) and one high-pressure (dashed line, labeled Hi P) crystallization path are shown for CaO/Al<sub>2</sub>O<sub>3</sub> (high-pressure path also calculated with procedure of Weaver and Langmuir [1990]). The line labeled “K&L” on the Na<sub>2</sub>O diagram is for MORB average from Klein and Langmuir (1987). Note that FeO\* values are recalculated from Fe<sub>2</sub>O<sub>3</sub>\* in Table 2.

flows are similar to one another. Average CaO/Al<sub>2</sub>O<sub>3</sub> also is similar for the two groups and, when plotted vs. Na<sub>8</sub> or Fe<sub>8</sub>, falls on the regionally averaged, global MORB array as well. Because Na<sub>8</sub>, Fe<sub>8</sub>, and CaO/Al<sub>2</sub>O<sub>3</sub> appear to reflect the integrated degree and depth of melting controlled by regional variations in the potential temperature of upwelling mantle (having homogeneous major element composition), these results indicate generally similar conditions of melting for Units A and C–G.

The position of the Site 807 data on the MORB array in Figure 11 is consistent with the hypothesis that the Ontong Java Plateau was formed near a spreading center; results for off-ridge hotspots and other magmatic settings often fall off the trend for regionally averaged

MORBs (e.g. Klein and Langmuir, 1987). Significantly, the Site 807 data plot at the low-Na<sub>8</sub>, high-Fe<sub>8</sub> end of the global MORB correlation; that is, at the end corresponding to the highest observed extents of partial melting. Indeed, their closest present-day analogs are Iceland and the Kolbeinsey and Reykjanes ridges flanking the Icelandic hotspot, a region characterized by notably greater degrees of melting than ordinary spreading centers far from hotspots (Dick et al., 1984; Klein and Langmuir, 1987). Lavas from the Nauru Basin adjacent to the plateau on the east have similar but slightly greater Na<sub>8</sub> and lesser Fe<sub>8</sub>, suggesting slightly lower extents of partial melting at the margins of the plateau. The ~90 Ma Site 803 basalts have low Na<sub>8</sub> but also lower Fe<sub>8</sub> than the Site 807 lavas; assuming the Site 803 samples give

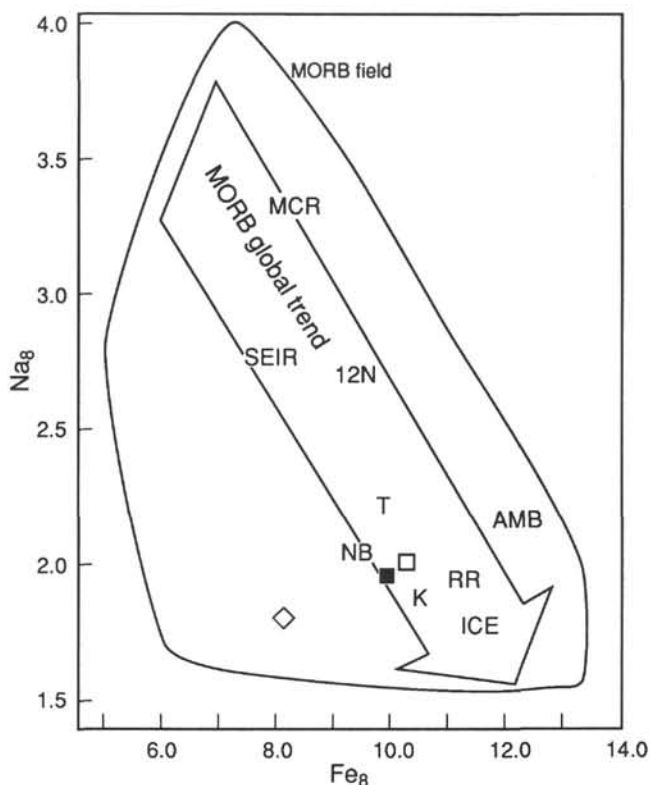


Figure 11. Average  $\text{Na}_8$  vs. average  $\text{Fe}_8$  for Site 807 Unit A (filled square) and Units C–G (open square), along with an outline of the overall field for MORB, an arrow representing the trend defined by regionally averaged MORB data, and average values for several specific present-day spreading centers (from Klein and Langmuir, 1987, 1989, and Klein et al., 1991) and Nauru Basin (NB; data from Castillo et al., 1986). ICE = Iceland, RR = Reykjanes Ridge, K = Kolbeinsey Ridge, T = Tamayo Fracture Zone, SEIR = eastern Southeast Indian Ridge, 12N = Mid-Atlantic Ridge 11.4°N–11.97°N, MCR = Mid-Cayman Rise. Note that Units A and C–G have similar average values and that both plot near the high-melting end of the global MORB array, along with ridges flanking the Icelandic hotspot. Site 803 (open diamond) has both low  $\text{Na}_8$  and low  $\text{Fe}_8$ . Also shown is a point for the Ambenali formation (AMB) of the Deccan Traps of India (from Z. Peng et al., unpubl. data, 1991).

a representative average for this site, they could reflect a high degree but shallower overall depth of melting than at Site 807. We also have included an average for the Deccan Traps of India (for the upper-level Ambenali formation, which is essentially uncontaminated by continental crust). This large flood basalt province appears to have been formed by the nascent Réunion hotspot (e.g., Morgan, 1981; Richards et al., 1989) in conjunction with continental rifting and the initiation of seafloor spreading above the hotspot about 66 Ma. Like the Ontong Java, the Ambenali plots relatively near the high-melting end of the MORB array; but neither the Deccan nor Ontong Java points lie at lower  $\text{Na}_8$  than data for Iceland or the Reykjanes Ridge. Thus, if the Ontong Java Plateau and the Deccan Traps reflect melting in the heads of new mantle plumes, these results provide no evidence for melting to an extent greater than occurs around a mature near-ridge plume tail such as Iceland.

Klein and Langmuir (1987) showed that, for their worldwide compilation of MORB data, reasonably good correlations exist between average regional  $\text{Na}_8$ ,  $\text{CaO}/\text{Al}_2\text{O}_3$ , and  $\text{Fe}_8$  vs. axial depth. When the average values of these chemical parameters for the Leg 130 rocks are plotted on the MORB correlations, they fall near the end of the MORB array corresponding to shallow axial depth, in the range for the Kolbeinsey and Reykjanes ridges. This result could be taken to imply a shallow eruption depth (less than about 1000 m) for the plateau

lavas. However, although parts of the plateau originally may have been at shallow levels, no evidence for such shallow paleodepths has been found at Sites 803, 807, or 289 or on southern Malaita; instead, the basement rocks and basal sediments sampled to date seem to indicate paleodepths of more than 1000 m (e.g., Kroenke, Berger, Janecek, et al., 1991). Some Leg 130 flows perhaps could have issued from distant eruptive vents at shallow depths (especially the thick Unit F), but many of the thin pillow lavas appear unlikely to have traveled very far. At present, we prefer not to draw any conclusions regarding paleodepths from the above petrochemical parameters. In particular, the Ontong Java Plateau could have been formed at least partly off-axis, but the correlations between eruption depth and  $\text{Na}_8$ ,  $\text{Fe}_8$ , and  $\text{CaO}/\text{Al}_2\text{O}_3$  hold only for axial lavas proper (Niu and Batiza, 1992); they do not obtain even for other near-ridge (but off-axis) basalts such as those on near-axis seamounts or flow fields; nor do they hold, in general, for intraplate basalts.

To provide somewhat more quantitative bounds on melting, the fractional melting inversion of M<sup>c</sup>Kenzie and O’Nions (1991) was applied. This inversion uses averaged rare-earth-element concentrations to estimate (1) melt distribution as a function of depth, (2) a total integrated melt fraction, and (3) equivalent crustal thickness corresponding to total melt produced. The rare-earth-element composition of the source, source mineralogy, and distribution coefficients for the rare earths are assumed, and fractional melting, rather than batch melting, is taken to be the operative process (as indeed is indicated by recent work on abyssal peridotites; Johnson et al., 1990). For this exercise, only data for samples with  $\text{MgO} > 6$  wt% were used (cf. M<sup>c</sup>Kenzie and O’Nions, 1991), and the data were averaged together irrespective of site (Leg 130 and Site 289) or stratigraphic location (Units A and C–G). Although Units A and C–G, for example, clearly had somewhat different mantle sources, averaging is reasonable because the total range of variation is small (e.g., only 1.4  $\epsilon_{\text{Nd}}$  units). The inversion was run on this average assuming mantle sources with either primitive or depleted (MORB mantle) rare-earth-element compositions.

Figure 12 illustrates the results (for the neutron activation data only) in the form of the concentration (normalized to assumed source) and melt fraction vs. depth diagrams used by M<sup>c</sup>Kenzie and O’Nions (1991). Individual points on Figures 12A and 12C are the normalized average concentrations of the data, with error bars indicating standard deviation for each element; the heavy solid line is the pattern determined by the inversion, with the lightly drawn solid and dashed lines representing estimated upper and lower limits. Both a MORB-type source and one with a primitive-mantle rare-earth pattern yield acceptable fits (i.e., the heavy solid line is close to the average value and well within the error bars for each rare-earth element). The primitive-source model produces a pattern with slightly greater light-rare-earth and slightly lower middle-rare-earth element abundances than the actual data, whereas the MORB-source model yields a pattern that is slightly lower in La and higher in Nd and Sm. In conjunction with the Nd isotopes, which require a source more enriched over time in the light rare earths than that of normal MORB, but less so than for primitive mantle, these results suggest that a mixed source is the most appropriate.

Estimated melt fraction as a function of depth is presented in Figures 12B and 12D. Here, the heavy dashed curve represents the calculated melt distribution after correction for crystal fractionation (the correction is based on the misfit between calculated and measured average  $\text{MgO}$  and total Fe as  $\text{FeO}$ , assumed to be caused by olivine fractionation; see M<sup>c</sup>Kenzie and O’Nions, 1991, for details). The heavy solid curve is the calculated distribution before the fractionation correction, and the lightly drawn lines the lower and upper limits. The fractionation correction is ~40%, owing to the evolved nature of the Leg 130 and Site 289 samples. Significantly, the estimated maximum melt fractions are very high for both the primitive- and MORB-source models, around 28%–30%, although melting of the primitive source begins at greater depth. The total thickness of melt produced

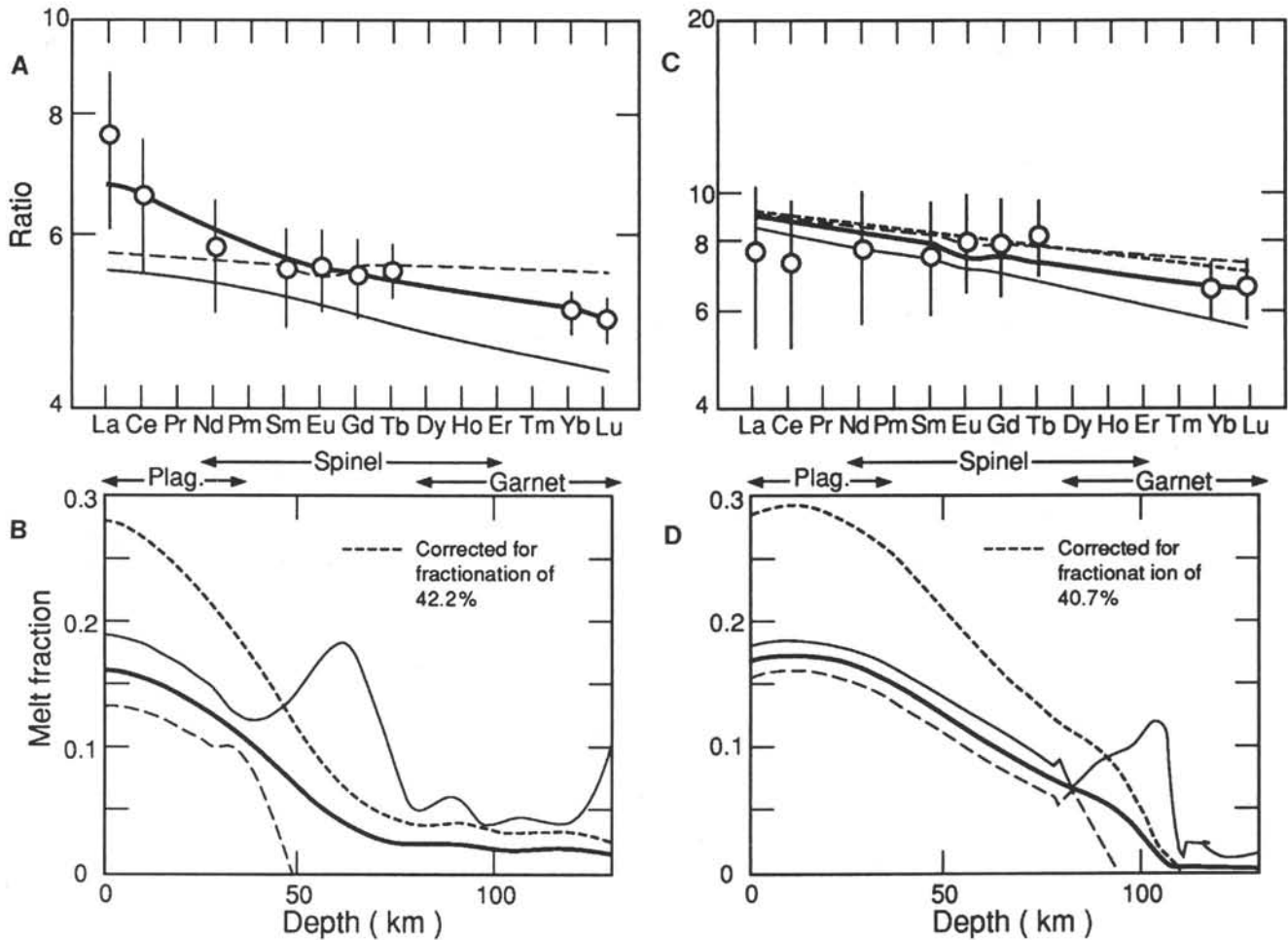


Figure 12. **A.** Element concentration ratio with respect to a normal-MORB mantle source (M<sup>c</sup>Kenzie and O’Nions, 1991) for average of Leg 130 and Site 289 basalts with MgO >6 wt% (average of neutron activation data only). Error bars indicate standard deviation of data for each element. The heavy solid line shows the rare earth pattern determined by fractional-melting inversion; the fine continuous and dashed lines represent patterns calculated from the estimated upper and lower bounds (see M<sup>c</sup>Kenzie and O’Nions, 1991 for details). Observed and calculated major element values (normalized to 100 wt% without K<sub>2</sub>O and P<sub>2</sub>O<sub>5</sub>) are given below; fractionation correction is calculated from the difference between observed and calculated MgO and FeO.

	SiO <sub>2</sub>	TiO <sub>2</sub>	Al <sub>2</sub> O <sub>3</sub>	FeO	MgO	CaO	Na <sub>2</sub> O	K <sub>2</sub> O
Obs.	50.37	1.33	14.61	11.63	7.40	12.36	2.30	0.16
±	0.59	0.22	0.44	0.93	0.62	0.32	0.17	0.10
Calc.	50.24	1.24	15.10	8.67	11.33	11.14	2.28	0.26
±	0.81	0.24	0.93	0.97	1.00	1.07	0.29	0.23
(Obs. - Calc.) S.D.	0.13	0.27	-0.48	2.20	-3.34	1.10	0.07	

**B.** Melt fraction (by weight) with depth calculated before (heavy continuous line) and after (heavy dashed line) correction for crystal fractionation. Fine dashed and continuous lines again represent the estimated lower and upper limits, respectively. Total melt thickness calculated from the inversion is 17.2 km after fractionation correction. **C, D.** Same as Figures 12A and 12B except for a primitive mantle source. Here the estimated total melt thickness after the fractionation correction is 24.3 km. Calculated major element values and difference between observed and calculated values are given below.

	SiO <sub>2</sub>	TiO <sub>2</sub>	Al <sub>2</sub> O <sub>3</sub>	FeO	MgO	CaO	Na <sub>2</sub> O	K <sub>2</sub> O
Calc.	49.82	1.08	14.81	9.00	12.10	11.05	2.15	0.26
±	0.81	0.24	0.93	0.97	1.00	1.07	0.29	0.23
(Obs. - Calc.) S.D.	0.55	0.75	-0.19	1.96	-3.99	1.17	0.46	

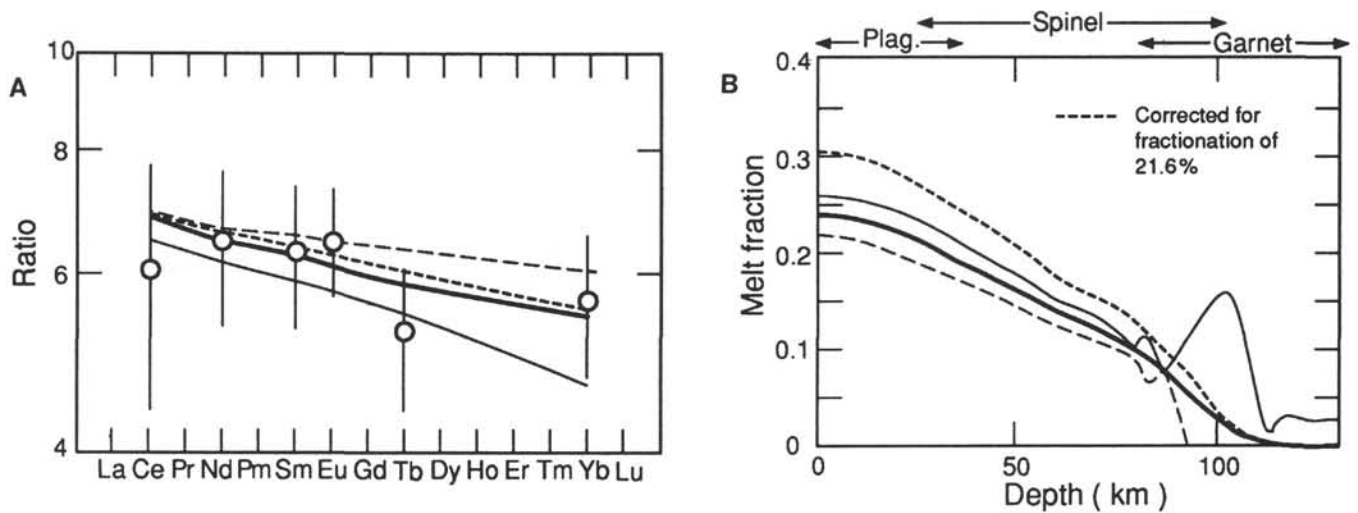


Figure 13. Results of inversion model for Manihiki Plateau lavas from Site 317, using data from Jackson et al. (1976), Mahoney (1987), and this paper (Table 3). See caption to Figure 12 and text for explanation. Here, Hf and Ti were used in addition to rare earths. Calculated total melt thickness is 23.7 km after fractionation correction of 21.6%. Observed and calculated major element concentrations are given below.

	SiO <sub>2</sub>	TiO <sub>2</sub>	Al <sub>2</sub> O <sub>3</sub>	FeO	MgO	CaO	Na <sub>2</sub> O	K <sub>2</sub> O
Obs.	51.27	1.00	15.61	9.81	8.45	11.65	2.21	0.07
±	0.36	0.06	0.21	0.38	0.64	0.14	0.08	0.04
Calc.	49.84	0.91	14.34	9.14	12.79	11.01	1.97	0.25
±	0.81	0.24	0.93	0.97	1.00	1.07	0.29	0.23
(Obs. - Calc.) S.D.	1.61	0.33	1.34	0.64	-3.65	0.59	0.82	

source models, around 28%-30%, although melting of the primitive source begins at greater depth. The total thickness of melt produced in the primitive-source model (after the fractionation correction) is 24.3 km; for the MORB-source model, it is 17.2 km. Results obtained by M<sup>c</sup>Kenzie and O'Nions (1991) for enriched MORBs from Iceland are remarkably similar: total amount of partial melt = ~30%; equivalent crustal thickness = 22.3 km for a primitive-source model after a 39% fractionation correction; and melt distribution with depth much like that for the Ontong Java primitive-source model. The estimated maximum (fractionation-corrected) extent of melting for normal MORBs, on the other hand, is only around 15%, and predicted crustal thickness is 9 km or less (M<sup>c</sup>Kenzie and O'Nions, 1991).

As a comparison to the Ontong Java case, the inversion also was applied to Manihiki Plateau data for DSDP Site 317. The Site 317 basalts exhibit a greater range of  $\epsilon_{Nd}$  than the Leg 130 rocks, but suitably comprehensive chemical analyses are available for only seven of the ten flows drilled, and only six rare-earth elements have been measured for most of them; therefore, the data were averaged and Hf and Ti, for which there are good measurements, were included in the inversion. Figure 13 presents the results. Not surprisingly, the variance associated with most of the rare-earth elements is greater than for the Ontong Java rocks, and Tb appears to be systematically low compared with the other rare earths; however, a primitive-source model produces an acceptable fit (though not shown graphically, the deviation for Ti and Hf is much smaller than for any of the rare-earth elements). Estimated total melt fraction and crustal thickness are again large at ~30% and 23.7 km, respectively, very similar to the results for the Ontong Java Plateau and Iceland (the fractionation correction here is only 22%, however, as the Site 317 lavas are relatively undifferentiated).

In short, the Ontong Java and Manihiki Plateau basalts appear to represent very high-degree melts with affinities to present-day lavas

from the vicinity of Iceland. The above results support a near-ridge hotspot or plume-head origin for the two Pacific plateaus. A completely off-ridge, plume-head origin would appear to be possible only with very substantial lithospheric thinning above the head (i.e., localized rifting that may not have linked up with a spreading center), or if the potential temperature (e.g., M<sup>c</sup>Kenzie and Bickle, 1988) in the head was sufficiently above that now beneath Iceland to produce comparably high-degree melts with lesser amounts of thinning. Although good evidence exists that the Manihiki Plateau formed at a ridge crest (Winterer et al., 1974; Sharman and Mammerickx, 1990), tectonic evidence for the original setting of the Ontong Java Plateau is somewhat more equivocal. The plateau is isostatically compensated and its structural features are consistent with a spreading center origin (e.g., Kroenke, 1972), but seafloor magnetic lineations to the east of Sites 807 and 289 (Larson, Schlanger, et al., 1981) are >25 m.y. older than the lavas at these drill sites. The lineations decrease in age to the south such that, if east-west continuity of the seafloor is assumed, the southern parts of the plateau (such as Malaita and the eastern lobe) may be the same age as the ocean crust to the east. However, the lineations cannot be traced westward beyond the edge of the plateau; instead, structural trends and a weak magnetic fabric on the plateau are oriented at an angle to those of the seafloor on the east, possibly indicating a major offset in the paleo-Pacific ridge system (e.g., Kroenke, 1972).

It is interesting that no indication, from either the major elements or inversion results, is evident of melting to an extent exceeding that observed today around Iceland, as has been proposed to exist near the axes of large plume heads (e.g., Campbell and Griffiths, 1990). (Based on their high-Cr spinels, near-primitive Manihiki Plateau dredge samples studied by Clague [1976] and Dick and Bullen [1984] may be an exception; the near-primary picrites of Curacao and the komatiitic lavas on the island of Gorgona, both probable fragments of the

Caribbean Plateau [Storey et al., 1991], may be another.) The Ontong Java lavas sampled so far, of course, simply may not correspond to the axial region of a plume head. Perhaps more serious is that the crustal thicknesses estimated by the inversion model, though considerable and, indeed, in the range of values estimated for the Kerguelen Plateau (e.g., Houtz et al., 1977), are significantly less than those actually measured for the Ontong Java Plateau by seismic refraction (30–40 km, with an average of ~36 km; Furumoto et al., 1976; Hussong et al., 1979). Assuming that both the model prediction and the refraction measurements are accurate, the difference may be because the available samples are not truly representative of the plateau's crust; in particular, they clearly record only the final episodes of volcanism, at least locally. Earlier, deeper parts of the crustal section might reflect even greater degrees of melting (cf. Storey et al., 1991) corresponding to greater crustal thicknesses. Also, if parts of the plateau were built on pre-existing oceanic crust, an extra 5–8 km can be added to the calculated (melt) thickness. In addition, some crustal thickening could have occurred after eruption of the sampled surface lavas, through underplating and intrusion.

### Relation of Site 803 Basalts to Other Sites

The plume-initiation model predicts a very short span of basement ages (only a few million years) across the plateau (e.g., Richards et al., 1989). Our early Aptian  $^{40}\text{Ar}$ - $^{39}\text{Ar}$  dates for Sites 807 and 289, and the preliminary results for Malaita (122–123 Ma; R.A. Duncan, unpubl. data, 1991) are essentially identical and thus strongly support the model. Likewise, although basement was not reached at DSDP Site 288, the oldest sediments recovered were Aptian (112–124.5 Ma; Harland et al., 1990), indicating that local basement is Aptian or older (Packham and Andrews, 1975). On the other hand, the three  $^{40}\text{Ar}$ - $^{39}\text{Ar}$  plateau ages obtained for Site 803 demonstrate that volcanism occurred there some 30 m.y. after it had ceased at Site 807. Whether appreciable amounts of plateau construction took place over a period of more than 30 m.y., or whether, for example, the 26 m of lavas penetrated at Site 803 represent only a brief local reactivation of volcanism long after most of the crust was emplaced around ~122 Ma cannot be determined conclusively at present, given so few basement sites (all with shallow penetration) over such a great area. Evidence is present of at least limited activity elsewhere on the plateau around 88–95 Ma, as recorded by volcanoclastic beds of Coniacian through mid-Cenomanian age at DSDP Site 288, which lies nearly 1000 km south of Site 803; also, somewhat older volcanoclastic layers of late Aptian to Albian age occur above basement at DSDP Site 289 (Packham and Andrews, 1975). What is clear from the present study is that the *end* of basalt eruption at several widely spaced locations was virtually contemporaneous in the early Aptian. Furthermore, the lack of any post-Aptian, Early Cretaceous ash layers or sills above basement at Site 807 and on Malaita (e.g., Packham and Andrews, 1975; Hughes and Turner, 1977) suggests that volcanism in the 120–90 Ma range, although present in places, was not particularly vigorous or widespread.

For the Manihiki Plateau, only basalts from Site 317 have been dated, yielding a weighted  $^{40}\text{Ar}$ - $^{39}\text{Ar}$  plateau age of  $123 \pm 1.5$  Ma (R.A. Duncan, unpubl. data, 1991). Basement ages have been obtained for several locations on the Kerguelen Plateau and Broken Ridge; they are remarkably similar to those for the Ontong Java both in absolute value and in total duration encompassed. Ages for the southern and central Kerguelen Plateau are between 110 and 118 Ma (Leclaire et al., 1987; Duncan, 1991; Whitechurch et al., 1992), whereas several lavas from Broken Ridge—originally contiguous with the central part of the Kerguelen Plateau—are 83–88 Ma (Duncan, 1991). Therefore, despite being separated by considerable distances, construction of all three of these large oceanic plateaus appears to have overlapped in time, as also inferred by Tarduno et al. (1991) on the basis of biostratigraphic dates of basal sediments. Moreover, on the only two plateaus where sampling has been done at several sites, a ca. 30-m.y.

record of volcanic activity has emerged. Unfortunately, the number of dated basement sites is as yet too small to construct a credible plot of erupted volume vs. age for any plateau. In the case of the Ontong Java, however, the present results suggest that the great bulk of edifice building may have transpired in a very short period around 122 Ma. If true, the plateau marks the largest igneous event in the last 200 m.y.

The ~30-m.y. span of ages for samples from the Kerguelen Plateau and Broken Ridge is consistent with a northward-younging age progression expected from the migration of the Antarctic Plate over the youthful Kerguelen hotspot (Duncan, 1991). For the Ontong Java Plateau, however, the ages of the widely dispersed Site 807, Site 289, and southern Malaitan locations are identical within errors, whereas Site 803, with a much younger age, sits at a latitude between Sites 807 and 289. Thus, no indication exists for any simple age progression across the plateau, and the roughly 90 Ma event recorded at Site 803 could have been imposed on the plateau after most of it was built. Volcanism of this age is observed throughout much of the western Pacific (Rea and Vallier, 1987; Winterer et al., unpubl. data, 1991) and may reflect a plate-wide extensional regime that resulted from a major change in the direction of plate motion. That similar ages mark the formation of Broken Ridge on the northeastern side of the Kerguelen Plateau could indicate that this reorganization was global in scope.

The geochemical information for Site 803 is surprising in view of the  $^{40}\text{Ar}$ - $^{39}\text{Ar}$  ages because, as noted above, the lavas isotopically resemble the lower units at Site 807 and the basalt at Site 289. They also possess very similar incompatible-element characteristics (Zr/Nb, La/Sm, Th/Ta, etc.; see Fig. 6), and like the basalts at the other sites, are olivine- or quartz-normative tholeiites. In other words, the mantle source and petrogenesis of lavas at Site 803 appear to have been much like those in the other, older locations. These features are contrary to what would be expected if, for instance, the Site 803 rocks reflected late-stage, small-degree remelting of older plateau lithosphere or nonplume asthenosphere (such as the unusual 34-Ma alnoite intrusions of Malaita appear to represent; e.g., Neal and Davidson, 1989), or the influence of a second hotspot overridden by the plateau at 90 Ma. As we have no reason to doubt the general validity of the  $^{40}\text{Ar}$ - $^{39}\text{Ar}$  ages for Site 803, the simplest explanation of the geochemical results is that the plateau was underlain by isotopically similar, hot plume-type mantle for at least 30 m.y. or passed over the same hotspot twice.

### Louisville Hotspot Connection

Not all plate reconstructions place the original location of the Ontong Java Plateau as far south as the Louisville hotspot (Yan and Kroenke, this volume), but several suggest that the plateau was near the hotspot around 120 Ma (see Richards et al., 1989; Mahoney and Spencer, 1991; Tarduno et al., 1991; and references therein). Because our  $^{40}\text{Ar}$ - $^{39}\text{Ar}$  ages for Sites 289 and 807 (as well as data for Malaita) are very close to this value, they offer general support for a Louisville hotspot source for the plateau. Isotopic fields for the 0–70 Ma seamounts of the Louisville Ridge are even more restricted than those of the Ontong Java basalts, and their initial Nd and Sr isotopic ratios are similar to those of Units C–G, Site 289, and Site 803. However, the Louisville Ridge has much higher  $^{206}\text{Pb}/^{204}\text{Pb}$  (19.1–19.5; Cheng et al., 1987) than any of the analyzed plateau lavas (Figs. 7, 8B, and 8C), even after allowance is made for age differences. If the Louisville hotspot was, in fact, the principal source of Ontong Java magmas, could the difference in Pb isotopes be a consequence of the evolution of Pb by radiogenic ingrowth in the plume? Pb abundances have not been determined for Louisville Ridge samples, but rather typical ocean-island-like  $^{238}\text{U}/^{204}\text{Pb}$  values of ~15–35 are indicated by their measured U and Ce abundances (Hawkins et al., 1987), assuming that Ce/Pb is relatively constant (Hofmann et al., 1986). Yet for the Louisville Ridge mantle source to evolve from the initial  $^{206}\text{Pb}/^{204}\text{Pb}$

of Site 803 at 90 Ma, for example, to the 70–0 Ma values of the ridge lavas would require much higher  $^{238}\text{U}/^{204}\text{Pb}$  in the source, from ~60 to more than 200, for which no evidence is present. Moreover, no systematic variation of  $^{206}\text{Pb}/^{204}\text{Pb}$  with age exists along the ridge itself. Of course, a wider range of isotopic values may eventually be found on the plateau and possibly along the Louisville Ridge as well; but it is worth pointing out that the latter data set covers the entire ~70-m.y. length of the seamount chain. Accepting a Louisville hotspot model for the plateau, the implication (assuming the existing Louisville Ridge isotopic field indeed is representative) is that products of the hotspot changed markedly in isotopic composition sometime between about 70 and 90 Ma, apparently losing an early, relatively low  $^{206}\text{Pb}/^{204}\text{Pb}$  fingerprint. Unfortunately, samples—or seamounts—from the 70–90 Ma period are not available to document such a shift, having been subducted beneath the Australian Plate. Notably, this change cannot be explained by a decrease in the contribution of Pacific MORB-type mantle to the hotspot, in contrast to temporal isotopic variations associated with, for example, the Réunion hotspot (White et al., 1990).

The apparent shift to higher  $^{206}\text{Pb}/^{204}\text{Pb}$  between the plateau and subsequent seamount chain could reflect a loss of low  $^{206}\text{Pb}/^{204}\text{Pb}$  mantle in the hotspot itself, or conceivably only a loss of the ability to melt such material. In a study of Indian Ocean MORB, Mahoney et al. (1989) suggested that low  $^{206}\text{Pb}/^{204}\text{Pb}$  mantle might be widely present in the Indian MORB source but be relatively refractory. Similarly, refractory low  $^{206}\text{Pb}/^{204}\text{Pb}$  material could have persisted in the Louisville plume but the extent of melting in the last 70 m.y. (after the plume-head and/or near-ridge stage) might not have been great enough for it to be expressed significantly. Much-diminished extents of melting are in fact indicated by the Louisville Ridge lavas, which, in contrast to the high-degree plateau melts, are alkalic basalts, hawaiites, and basanitoids representing degrees of melting estimated in the 4%–9% range (Hawkins et al., 1987). A sustained, substantially lower overall amount of melting also is implied by the total volume of the seamount chain, which is very small ( $\sim 2 \times 10^5 \text{ km}^3$ ; Lonsdale, 1988) compared with that of the plateau ( $\sim 5 \times 10^7 \text{ km}^3$ ; Mahoney, 1987).

Additional evidence exists elsewhere for an early expression of low  $^{206}\text{Pb}/^{204}\text{Pb}$  compositions not found in later products of a hotspot. In the Kerguelen system, the lowest  $^{206}\text{Pb}/^{204}\text{Pb}$  values (to 17.47) occur only among the Early Cretaceous lavas of the southern Kerguelen Plateau and not in the sampled portions of the subsequent hotspot track, which predominantly have  $^{206}\text{Pb}/^{204}\text{Pb} > 17.9$  (as do many of the early plateau lavas also) (e.g., Storey et al., 1989, 1992; Weis et al., 1989; Barling and Goldstein, 1990; Weis and Frey, 1991; Saunders et al., 1991). The Manihiki Plateau is not linked with certainty to any hotspot, but paleoceanographic reconstructions indicate that it originally lay in the southeast Pacific; none of the present hotspots in this region, with which it has sometimes been associated (Juan Fernandez, Easter, San Felix), have  $^{206}\text{Pb}/^{204}\text{Pb}$  nearly as low as the Site 317 basalts (Mahoney and Spencer, 1991). Again, in the Tristan hotspot system (Paraná flood basalts, Walvis Ridge, Rio Grande Rise, Tristan da Cunha, and Gough islands), by far the lowest Pb isotopic ratios measured (to 17.1) are in the early products of the hotspot, the ~130-Ma high phosphorus and titanium (HPT) flood basalts (e.g., Hawkesworth et al., 1986); the same may be true of the Marion hotspot system (Mahoney et al., 1991).

In the Paraná, Kerguelen, and possibly Marion examples, the early low  $^{206}\text{Pb}/^{204}\text{Pb}$  signatures could be caused by plume-induced melting of continental lithosphere, the availability of which decreased as the continents drifted away from the hotspots (e.g., Storey et al., 1992). Such a mechanism is far less probable for the intraoceanic Ontong Java and Manihiki plateaus, where low  $^{206}\text{Pb}/^{204}\text{Pb}$  mantle would more likely be indigenous to the plume. In either case, however, the loss of low  $^{206}\text{Pb}/^{204}\text{Pb}$  characteristics could be a result of the decreasing ability of a plume to melt refractory mantle (whether originally continental or not), either as the plume's distance from a rift or

spreading center increased (and hence the amount of decompressional melting was reduced; e.g., McKenzie and Bickle, 1988) or as it went from an expanded plume-head to a restricted plume-tail stage. The Hawaiian example provides a possible argument against this hypothesis because both low  $^{206}\text{Pb}/^{204}\text{Pb}$  (~17.7) and higher  $^{206}\text{Pb}/^{204}\text{Pb}$  (~18.6) components are present in recent Hawaiian shield volcanoes (e.g., West et al., 1987), but the shields possessing the lowest  $^{206}\text{Pb}/^{204}\text{Pb}$  signatures are not the largest ones (Bargar and Jackson, 1976). For the present, therefore, we suggest the above idea only as a possibility.

## CONCLUSIONS

The Ontong Java Plateau probably represents an early stage of a hotspot, possibly the Louisville hotspot, and very likely corresponds to its initial plume-head phase. Supporting this conclusion are the  $^{40}\text{Ar}/^{39}\text{Ar}$  ages for basement at Sites 807 and 289, and preliminary data for Malaita (all 120–124 Ma), which (1) show that volcanism ceased in a period of only a few million years at several widely spaced locations across the plateau, and (2) are consistent with recent plate reconstructions placing it near the Louisville hotspot at this time. Moreover, Ontong Java lavas appear to represent very high-degree melts; their closest analogs today are found around Iceland, a vigorous near-ridge hotspot, consistent with a near-ridge origin for the plateau. The plateau could at least partly have formed in an off-axis setting, however, if lithospheric thinning induced by the plume head was substantial enough and/or the plume head was sufficiently hot enough to cause extents of partial melting comparable with those in Iceland. No evidence exists for a monotonic north-south age progression across the plateau; however, at least some activity continued to ~90 Ma, as recorded by basement at Site 803 and late Aptian to Coniacian volcanoclastic layers at Sites 288 and 289. Because the plume-initiation model predicts that plateaus are constructed in only a few million years, the measured span of more than 30 m.y. suggests that the model should be embraced with some caution—at least in its details. Presumably, the bulk of such an edifice can be built rapidly, but if it remains within the vicinity of hot plume mantle, some volcanism may continue for an extended period or be reactivated by favorable plate-tectonic developments.

Isotopically and chemically, the Leg 130 rocks are very similar to those previously analyzed from Site 289 and southern Malaita, but they are distinct from 0 to 70 Ma lavas of the Louisville hotspot's trace, the Louisville Ridge. Accepting a Louisville source for the plateau, the isotopic data suggest a shift of hotspot compositions to significantly higher  $^{206}\text{Pb}/^{204}\text{Pb}$  sometime between 70 and 90 Ma, possibly coincident with the transition from the plume-head to plume-tail stage of the hotspot's development. A similar loss of early low  $^{206}\text{Pb}/^{204}\text{Pb}$  compositions is seen in several other plateau-hotspot or continental flood basalt-hotspot systems; it could reflect a loss of low  $^{206}\text{Pb}/^{204}\text{Pb}$  mantle in (or in contact with) the plume, or an inability of at least some off-ridge plume tails to melt refractory low  $^{206}\text{Pb}/^{204}\text{Pb}$  material.

Finally, our results neither particularly support nor discredit the recent "superplume" hypothesis (Larson, 1991). However, because our age data and most recent plate reconstructions generally bolster a connection between the plateau and the present Louisville hotspot, we see no need, at present, to appeal to an oceanwide superplume to explain the Ontong Java Plateau.

## ACKNOWLEDGMENTS

We are grateful to Dan McKenzie for invaluable help with his inversion procedure; to Peter Floyd for supporting M. Storey during the early part of the study; to David Emley, who assisted with the XRF analyses; and to Andy Saunders for the NAA data. Nancy Hulbert illustrated the figures, and Carol Koyanagi got the text and tables into respectable shape. We thank reviewers A. Saunders and C. Neal; Bill

White and Pat Castillo also provided helpful comments. This research was supported by NSF grant ODP-TAMRF 20477, by the University of Keele, and by the NERC. This is SOEST Contribution No. 2702.

## REFERENCES

- Baksi, A.K., 1989. Reevaluation of the timing and duration of extrusion of the Imnaha, Picture Gorge and Grande Ronde Basalt. *Spec. Pap.-Geol. Soc. Am.*, 239:105-111.
- Bargar, K.E., and Jackson, E.D., 1976. Calculated volumes of individual shield volcanoes along the Hawaiian-Emperor chain. *J. Res. U.S. Geol. Surv.*, 2:545-551.
- Barling, J., and Goldstein, S.L., 1990. Extreme isotopic variations in Heard Island lavas and the nature of mantle reservoirs. *Nature*, 348:59-62.
- Bender, J.F., Hodges, F.N., and Bence, A.E., 1978. Petrogenesis of basalts from the Project FAMOUS area: experimental study from 0 to 15 Kbars. *Earth Planet. Sci. Lett.*, 41:277-302.
- Campbell, I.H., and Griffiths, R.W., 1990. Implications of mantle plume structure for the evolution of flood basalts. *Earth Planet. Sci. Lett.*, 99:79-93.
- Castillo, P., Batiza, R., and Stern, R.J., 1986. Petrology and geochemistry of Nauru Basin igneous complex: large volume, off-ridge eruptions of MORB-like basalt during the Cretaceous. In Moberly, R., Schlanger, S.O., et al., *Init. Repts. DSDP*, 89: Washington (U.S. Govt. Printing Office), 555-576.
- Castillo, P.R., Carlson, R.W., and Batiza, R., 1991. Origin of Nauru Basin igneous complex: Sr, Nd, and Pb isotopes and REE constraints. *Earth Planet. Sci. Lett.*, 103:200-213.
- Chaffey, D.J., Cliff, R.A., and Wilson, B.M., 1989. Characteristics of the St. Helena magma source. In Saunders, A.D., and Norry, M.J. (Eds.), *Magmatism in the Ocean Basins. Geol. Soc. Spec. Publ. London*, 42:257-276.
- Cheng, Q., Park, K.-H., Macdougall, J.D., Zindler, A., Lugmair, G.W., Hawkins, J., Lonsdale, P., and Staudigel, H., 1987. Isotopic evidence for a hot spot origin of the Louisville seamount chain. In Keating, B., Fryer, P., Batiza, R., and Boehlert, G. (Eds.), *Seamounts, Islands, and Atolls. Am. Geophys. Union Monogr.*, 43:283-296.
- Clague, D.A., 1976. Petrology of basaltic and gabbroic rocks dredged from the Danger Island Troughs, Manihiki Plateau. In Schlanger, S.O., Jackson, E.D., et al., *Init. Repts. DSDP*, 33: Washington (U.S. Govt. Printing Office), 891-911.
- Courtillot, V., Feraud, G., Maluski, H., Vandamme, D., Moreau, M.G., and Besse, J., 1988. Deccan flood basalts and the Cretaceous/Tertiary boundary. *Nature*, 333:843-846.
- Dalrymple, G.B., Lanphere, M.A., and Clague, D.A., 1981. Conventional and  $^{40}\text{Ar}/^{39}\text{Ar}$  K-Ar ages of volcanic rocks from Ojin (Site 430), Nintoku (Site 432), and Suiko (Site 433) seamounts and the chronology of volcanic propagation along the Hawaiian-Emperor chain. In Jackson, E.D., Koizumi, I., et al., *Init. Repts. DSDP*, 55: Washington (U.S. Govt. Printing Office), 659-676.
- Dick, H.J.B., and Bullen, T., 1984. Chromium spinel as a petrogenetic indicator in abyssal and alpine-type peridotites and spatially-associated lavas. *Contrib. Mineral. Petrol.*, 86:54-76.
- Dick, H.J.B., Fisher, R.L., and Bryan, W.B., 1984. Mineralogic variability of the uppermost mantle along mid-ocean ridges. *Earth Planet. Sci. Lett.*, 69:88-106.
- Duncan, R.A., 1991. Age distribution of volcanism along aseismic ridges in the eastern Indian Ocean. In Weissel, J., Peirce, J., Taylor E., Alt, J., et al., *Proc. ODP, Sci. Results*, 121: College Station, TX (Ocean Drilling Program), 507-518.
- Duncan, R.A., and Pyle, D.G., 1988. Rapid eruption of the Deccan flood basalts at the Cretaceous/Tertiary boundary. *Nature*, 333:841-843.
- Floyd, P.A., 1986. Petrology and geochemistry of oceanic intraplate sheet-flow basalts. Nauru Basin, Deep Sea Drilling Project, Leg 89. In Moberly, R., Schlanger, S.O., et al., *Init. Repts. DSDP*, 89: Washington (U.S. Govt. Printing Office), 471-497.
- Furumoto, A.S., Webb, J.P., Odegard, M.E., and Hussong, D.M., 1976. Seismic studies on the Ontong Java Plateau, 1970. *Tectonophysics*, 34:71-90.
- Govindaraju, K., 1989. 1989 compilation of working values and sample descriptions for 272 geostandards. *Geostandards Newsl.*, No. 13 (spec. issue).
- Hanan, B.B., and Schilling, J.-G., 1989. Easter microplate evolution: Pb isotope evidence. *J. Geophys. Res.*, 94:7432-7448.
- Hanson, G.N., 1980. Rare-earth elements in petrogenetic studies of igneous systems. *Annu. Rev. Earth Planet. Sci.*, 8:371-406.
- Harland, W.B., Armstrong, R.L., Cox, A.V., Craig, L.E., Smith, A.G., and Smith, D.G., 1990. *A Geologic Time Scale 1989*: Cambridge (Cambridge Univ. Press).
- Hart, S.R., 1988. Heterogeneous mantle domains: signatures, genesis and mixing chronologies. *Earth Planet. Sci. Lett.*, 90:273-296.
- Hawkesworth, C.J., Kempton, P.D., Rogers, N.W., Ellam, R.M., and van Calsteren, P.W., 1990. Continental mantle lithosphere, and shallow level enrichment processes in the Earth's mantle. *Earth Planet. Sci. Lett.*, 96:256-268.
- Hawkesworth, C.J., Mantovani, M.S.M., Taylor, P.N., and Palacz, Z., 1986. Evidence from the Paraná of South Brazil for a continental contribution to Dupal basalts. *Nature*, 322:356-359.
- Hawkins, J.W., Lonsdale, P.F., and Batiza, R., 1987. Petrologic evolution of the Louisville seamount chain. In Keating, B., Fryer, P., Batiza, R., and Boehlert, G. (Eds.), *Seamounts, Islands, and Atolls. Am. Geophys. Union Monogr.*, 43:235-254.
- Hofmann, A.W., Jochum, K.P., Seufert, M., and White, W.M., 1986. Nb and Pb in oceanic basalts: new constraints on mantle evolution. *Earth Planet. Sci. Lett.*, 79:33-45.
- Houtz, R.E., Hayes, D.E., and Markl, R.G., 1977. Kerguelen plateau bathymetry, sediment distribution and crustal structure. *Mar. Geol.*, 25:95-130.
- Hughes, G.W., and Turner, C.C., 1977. Upraised Pacific Ocean floor, southern Malaita, Solomon Islands. *Geol. Soc. Am. Bull.*, 88:412-424.
- Hussong, D.M., Wipperfurth, L.K., and Kroenke, L.W., 1979. The crustal structure of the Ontong Java and Manihiki oceanic plateaus. *J. Geophys. Res.*, 84:6003-6010.
- Jackson, E.D., Bargar, K.E., Fabbri, B.P., and Heropoulos, C., 1976. Petrology of basaltic rocks drilled on Leg 33 of the Deep Sea Drilling Project. In Schlanger, S.O., Jackson, E.D., et al., *Init. Repts. DSDP*, 33: Washington (U.S. Govt. Printing Office), 571-630.
- Jenner, G.A., Longerich, H.P., Jackson, S.E., and Fryer, B.J., 1990. ICP-MS; a powerful tool for high-precision trace-element analysis in earth sciences: evidence from analysis of selected U.S.G.S. reference samples. *Chem. Geol.*, 83:133-148.
- Johnson, K.T., Dick, H.J.B., and Shimizu, N., 1990. Melting in the oceanic upper mantle: an ion microprobe study of diopsides in abyssal peridotites. *J. Geophys. Res.*, 95:2661-2678.
- Klein, E.M., and Langmuir, C.H., 1987. Global correlations of ocean ridge basalt chemistry with axial depth and crustal thickness. *J. Geophys. Res.*, 92:8089-8115.
- , 1989. Local versus global variations in ocean ridge basalt composition: a reply. *J. Geophys. Res.*, 94:4241-4252.
- Klein, E.M., Langmuir, C.H., and Staudigel, H., 1991. Geochemistry of basalts from the Southeast Indian Ridge, 115E-138E. *J. Geophys. Res.*, 96:2089-2107.
- Kroenke, L.W., 1972. Geology of the Ontong Java Plateau. *Hawaii Inst. Geophys. Rep. HIG*, 72-75.
- Kroenke, L.W., Berger, W.H., Janecsek, T.R., et al., 1991. *Proc. ODP, Init. Repts.*, 130: College Station, TX (Ocean Drilling Program).
- Lanphere, M.A., and Dalrymple, G.B., 1978. The use of  $^{40}\text{Ar}/^{39}\text{Ar}$  Ar data in evaluation of disturbed K-Ar systems. In Zartman, R.E. (Ed.), *Short Papers of the Fourth International Conference, Geochronology, Cosmochronology, Isotope Geology*. Open-File Rep., U.S. Geol. Surv., 78-701:241-243.
- Larson, R.L., 1991. Latest pulse of the Earth: evidence for a mid-Cretaceous super plume. *Geology*, 19:547-550.
- Larson, R.L., Schlanger, S.O., et al., 1981. *Init. Repts. DSDP*, 61: Washington (U.S. Govt. Printing Office).
- Leclaire, L., Bassias, Y., Denis-Clochchiatti, M., Davies, H., Gautier, I., Gensous, B., Giannesini, P.J., Patriat, P., Segoufin, J., Tesson, M., and Wannesson, J., 1987. Lower Cretaceous basalt and sediments from the Kerguelen Plateau. *Geo-Mar. Lett.*, 7:169-176.
- Lonsdale, P., 1988. Geography and history of the Louisville hotspot chain in the Southwest Pacific. *J. Geophys. Res.*, 93:3078-3104.
- Mahoney, J., Nicollet, C., and Dupuy, C., 1991. Madagascar basalts: tracking oceanic and continental sources. *Earth Planet. Sci. Lett.*, 104:350-363.
- Mahoney, J.J., 1987. An isotopic survey of Pacific oceanic plateaus: implications for their nature and origin. In Keating, B., Fryer, P., Batiza R., and Boehlert, G. (Eds.), *Seamounts, Islands, and Atolls. Am. Geophys. Union Monogr.*, 43:207-220.
- Mahoney, J.J., Natland, J.H., White, W.M., Poreda, R., Bloomer, S.H., Fisher, R.L., and Baxter, A.N., 1989. Isotopic and geochemical provinces of the western Indian Ocean spreading centers. *J. Geophys. Res.*, 94:4033-4053.

- Mahoney, J.J., and Spencer, K.J., 1991. Isotopic evidence for the origin of the Manihiki and Ontong Java oceanic plateaus. *Earth Planet. Sci. Lett.*, 104:196–210.
- McKenzie, D., and Bickle, M.J., 1988. The volume and composition of melt generated by extension of the lithosphere. *J. Petrol.*, 29:625–679.
- McKenzie, D., and O'Nions, R.K., 1991. Partial melt distributions from inversion of rare earth element concentrations. *J. Petrol.*, 32:1021–1091.
- Mehl, K.W., Bitschene, P.R., Schminke, H.-U., and Hertogen, J., 1991. Composition, alteration, and origin of the basement lavas and volcanoclastic rocks at Site 738, Southern Kerguelen Plateau. In Barron, J., Larsen, B., et al., *Proc. ODP, Sci. Results*, 119: College Station, TX (Ocean Drilling Program), 299–321.
- Morgan, W.J., 1981. Hotspot tracks and the opening of the Atlantic and Indian oceans. In Emiliani, C. (Ed.), *The Sea* (Vol. 7): New York (Wiley), 443–487.
- Musgrave, R.J., 1990. Palaeomagnetism and tectonics of Malaita, Solomon Islands. *Tectonics*, 9:735–760.
- Neal, C.R., and Davidson, J.P., 1989. An unmetasomatized source for the Malaitan alnoite (Solomon Islands): petrogenesis involving zone refining, megacryst fractionation, and assimilation of oceanic lithosphere. *Geochim. Cosmochim. Acta*, 53:1975–1990.
- Niu, Y., and Batiza, R., in press. Chemical variations at fast- and slow-spreading mid-ocean ridges: a diapiric melting model. *J. Geophys. Res.*
- Oskarsson, N., Steinthorsson, S., and Sigvaldason, G.E., 1985. Icelandic geochemical anomaly: origin, volcanotectonics, chemical fractionation, and isotope evolution of the crust. *J. Geophys. Res.*, 90:10011–10025.
- Packham, G., and Andrews, J.E., 1975. Results of Leg 30 and the geological history of the southwest Pacific arc and marginal sea complex. In Andrews, J.E., Packham, G., et al., *Init. Repts. DSDP*, 30: Washington (U.S. Govt. Printing Office), 691–706.
- Paul, D.K., and Potts, P.J., 1981. Rare-earth abundances and origin of some Indian lamprophyres. *Geol. Mag.*, 118:393–399.
- Prinzhofer, A., Lewin, E., and Allègre, C.J., 1989. Stochastic melting of the marble cake mantle: evidence from local study of the East Pacific Rise at 12°50'N. *Earth Planet. Sci. Lett.*, 92:189–206.
- Rea, D.K., and Vallier, T.L., 1987. Cretaceous volcanic episodes in the Pacific. *Geol. Soc. Am. Bull.*, 94:1430–1437.
- Renne, P.R., and Basu, A.R., 1991. Rapid eruption of the Siberian Traps flood basalts at the Permo-Triassic boundary. *Science*, 253:176–179.
- Richards, M.A., Duncan, R.A., and Courtillot, V., 1989. Flood basalts and hot-spot tracks: plume heads and tails. *Science*, 246:103–107.
- Salters, V.J.M., Storey, M., Sevigny, J.H., and Whitechurch, H., 1992. Trace element and isotopic characteristics of Kerguelen-Heard Plateau basalts. In Wise, S.W., Jr., Schlich, R., et al., *Proc. ODP, Sci. Results*, 120: College Station, TX (Ocean Drilling Program), 55–62.
- Samson, S.D., and Alexander, E.C., 1987. Calibration of the interlaboratory <sup>40</sup>Ar-<sup>39</sup>Ar dating standard, Mmhb-1. *Chem. Geol.*, 66:27–34.
- Saunders, A.D., 1986. Geochemistry of basalts from the Nauru Basin, Deep Sea Drilling Project Legs 61 and 89: implications for the origin of oceanic flood basalts. In Moberly, R., Schlanger, S.O., et al., *Init. Repts. DSDP*, 89: Washington (U.S. Govt. Printing Office), 499–518.
- Saunders, A.D., Storey, M., Gibson, I.L., Leat, P., Hergt, J., and Thompson, R.N., 1991. Chemical and isotopic constraints on the origin of basalts from Ninetyeast Ridge, Indian Ocean: results from DSDP Legs 22 and 26 and ODP Leg 121. *Proc. ODP, Sci. Results*, 121: College Station, TX (Ocean Drilling Program), 559–590.
- Sharman, G.F., and Mammerickx, J., 1990. Eastern boundary of the Manihiki Plateau: a propagating rift site. *Eos*, 71:1668.
- Staudigel, H., Park, K.-H., Pringle, M., Rubenstone, J.L., Smith, W.H.F., and Zindler, A., 1991. The longevity of the South Pacific isotope and thermal anomaly. *Earth Planet. Sci. Lett.*, 102:24–44.
- Stoeser, D.B., 1975. Igneous rocks from Leg 30 of the Deep Sea Drilling Project. In Andrews, J.E., Packham, G., et al., *Init. Repts. DSDP*, 30: Washington (U.S. Govt. Printing Office), 401–444.
- Storey, M., Kent, R.W., Saunders, A.D., Salters, V.J., Hergt, J., Whitechurch, H., Sevigny, J.H., Thirlwall, M.F., Leat, P., Ghose, N.C., and Gifford, M., 1992. Lower Cretaceous volcanic rocks on continental margins and their relationship to the Kerguelen Plateau. In Wise, S.W., Jr., Schlich, R., et al., *Proc. ODP, Sci. Results*, 120: College Station, TX (Ocean Drilling Program), 33–53.
- Storey, M., Mahoney, J.J., Kroenke, L.W., and Saunders, A.D., 1991. Are oceanic plateaus sites of komatiite formation? *Geology*, 19:376–379.
- Storey, M., Saunders, A.D., Tarney, J., Gibson, I.L., Norry, M.J., Thirlwall, M.F., Leat, P., Thompson, R.N., and Menzies, M.A., 1989. Contamination of Indian Ocean asthenosphere by the Kerguelen-Heard mantle plume. *Nature*, 338:574–576.
- Sun, S.-S., and McDonough, W.F., 1989. Chemical and isotopic systematics of oceanic basalts: implications for mantle composition and processes. In Saunders, A.D., and Norry, M.J. (Eds.), *Magmatism in the Ocean Basins*. Geol. Soc. Spec. Publ. London, 42:313–345.
- Tarduno, J.A., Sliter, W.V., Kroenke, L.W., Leckie, M., Mayer, H., Mahoney, J.J., Musgrave, R., Storey, M., and Winterer, E.L., 1991. Rapid formation of Ontong Java Plateau by Aptian mantle plume volcanism. *Science*, 254:399–403.
- Todt, W., Cliff, R.A., Hanser, H., and Hoffmann, A.W., 1984. <sup>202</sup>Pb + <sup>205</sup>Pb double spike for lead isotopic analyses. *Terra Cognita*, 4:209.
- Tokuyama, H., and Batiza, R., 1981. Chemical composition of igneous rocks and origin of the sill and pillow-basalt complex of Nauru Basin, southwest Pacific. In Larson, R.L., Schlanger, S.O., et al., *Init. Repts. DSDP*, 61: Washington (U.S. Govt. Printing Office), 673–687.
- Walker, D.A., and McDougall, I., 1982. <sup>40</sup>Ar/<sup>39</sup>Ar and K-Ar dating of altered glassy volcanic rocks: the Dabi Volcanics, P.N.G. *Geochim. Cosmochim. Acta*, 46:2181–2190.
- Weaver, B.L., Wood, D.A., Tarney, J., and Joron, J.-L., 1987. Geochemistry of ocean island basalts from the South Atlantic: Ascension, Bouvet, St. Helena, Gough and Tristan da Cunha. In Fitton, J.G., and Upton, B.G.J. (Eds.), *Alkaline Igneous Rocks*. Geol. Soc. Spec. Publ. London, 30:253–267.
- Weaver, J.S., and Langmuir, C.H., 1990. Calculation of phase equilibrium in mineral-melt systems. *Computers Geosci.*, 16:1–19.
- Weis, D., Bassias, Y., Gautier, I., and Mennessier, J.-P., 1989. Dupal anomaly in existence 115 Ma ago: evidence from isotopic study of the Kerguelen Plateau (South Indian Ocean). *Geochim. Cosmochim. Acta*, 53:2125–2131.
- Weis, D., and Frey, F.A., 1991. Isotope geochemistry of Ninetyeast Ridge basement basalts: Sr, Nd, and Pb evidence for involvement of the Kerguelen hot spot. In Weissel, J., Pierce, J., Taylor, E., Alt, J., et al., *Proc. ODP, Sci. Results*, 121: College Station, TX (Ocean Drilling Program), 591–610.
- West, H.B., Gerlach, D.C., Leeman, W.P., and Garcia, M.O., 1987. Isotope constraints on the origin of Hawaiian lavas from the Maui Volcanic Complex, Hawaii. *Nature*, 330:216–220.
- White, W.M., Cheatham, M.M., and Duncan, R.A., 1990. Isotope geochemistry of Leg 115 basalts and inferences on the history of the Réunion mantle plume. In Duncan, R.A., Backman, J., Peterson, L.C., et al., *Proc. ODP, Sci. Results*, 115: College Station, TX (Ocean Drilling Program), 53–61.
- White, W.M., Hofmann, A.W., and Puchelt, H., 1987. Isotope geochemistry of Pacific mid-ocean ridge basalt. *J. Geophys. Res.*, 92:4881–4893.
- Whitechurch, H., Montigny, R., Sevigny, J., Storey, M., and Salters, V., 1992. K-Ar and <sup>40</sup>Ar/<sup>39</sup>Ar ages of Central Kerguelen Plateau basalts. In Wise, S.W., Jr., Schlich, R., et al., *Proc. ODP, Sci. Results*, 120: College Station, TX (Ocean Drilling Program), 71–77.
- Winterer, E.L., Lonsdale, P.F., Matthews, J.L., and Rosendahl, B.R., 1974. Structure and acoustic stratigraphy of the Manihiki Plateau. *Deep-Sea Res.*, Pt. A, 21:793–814.
- York, D., 1969. Least-squares fitting of a straight line with correlated errors. *Earth Planet. Sci. Lett.*, 5:320–324.

**Date of initial receipt: 20 November 1991**

**Date of acceptance: 15 June 1992**

**Ms 130B-040**